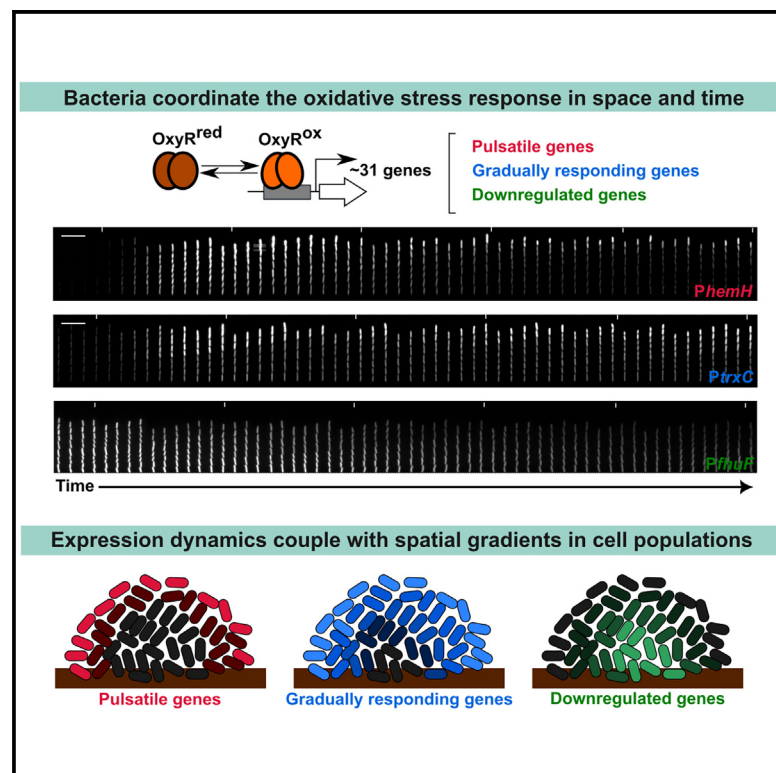


The master regulator OxyR orchestrates bacterial oxidative stress response genes in space and time

Graphical abstract



Authors

Divya Choudhary, Kevin R. Foster, Stephan Uphoff

Correspondence

kevin.foster@path.ox.ac.uk (K.R.F.), stephan.uphoff@bioch.ox.ac.uk (S.U.)

In brief

Bacteria rewire gene expression to survive stress, but the logic of these changes can remain elusive in bulk studies. Using single-cell imaging, Choudhary et al. reveal that the gene expression patterns under oxidative stress fall into three classes based on OxyR binding dynamics: downregulated, pulsatile, and gradually upregulated genes. Pulsatile genes provide initial protection by a few cells, whereas gradually upregulated genes ensure long-term defense across many cells. This reveals how bacterial populations coordinate stress responses in space and time.

Highlights

- Bacteria coordinate diverse oxidative stress response genes in space and time
- OxyR binding kinetics generate different induction or repression dynamics
- Expression dynamics are coupled with spatial gradients in cell populations
- Gene expression patterns relate to individual and collective cell behavior



Article

The master regulator OxyR orchestrates bacterial oxidative stress response genes in space and time

Divya Choudhary,¹ Kevin R. Foster,^{1,2,3,*} and Stephan Uphoff^{1,4,*}¹Department of Biochemistry, University of Oxford, Oxford, UK²Department of Biology, University of Oxford, Oxford, UK³Sir William Dunn School of Pathology, South Parks Road, Oxford OX1 3RE, UK⁴Lead contact*Correspondence: kevin.foster@path.ox.ac.uk (K.R.F.), stephan.uphoff@bioch.ox.ac.uk (S.U.)<https://doi.org/10.1016/j.cels.2024.10.003>

SUMMARY

Bacteria employ diverse gene regulatory networks to survive stress, but deciphering the underlying logic of these complex networks has proved challenging. Here, we use time-resolved single-cell imaging to explore the functioning of the *E. coli* regulatory response to oxidative stress. We observe diverse gene expression dynamics within the network. However, by controlling for stress-induced growth-rate changes, we show that these patterns involve just three classes of regulation: downregulated genes, upregulated pulsatile genes, and gradually upregulated genes. The two upregulated classes are distinguished by differences in the binding of the transcription factor, OxyR, and appear to play distinct roles during stress protection. Pulsatile genes activate transiently in a few cells for initial protection of a group of cells, whereas gradually upregulated genes induce evenly, generating a lasting protection involving many cells. Our study shows how bacterial populations use simple regulatory principles to coordinate stress responses in space and time. A record of this paper's transparent peer review process is included in the supplemental information.

INTRODUCTION

Bacterial stress response regulons are highly complex in that they commonly involve a suite of genes performing diverse functions, which display a variety of expression patterns under stress.¹ However, these regulons are also typically under the control of a single master transcriptional regulator. This begs the question of how such simple regulation is able to orchestrate the timing and magnitude of so many genes. Bulk transcriptomic and proteomic studies have documented an association between stress tolerance and gene regulation for a wide range of stresses, including under starvation,^{2,3} oxidative stress,⁴ osmotic stress,⁵ heat stress,^{5,6} pH stress,⁷ DNA damage,^{8,9} phage infection,¹⁰ and antibiotic exposure.¹¹ Moreover, these methods often identify tens to hundreds of genes that shift in expression with stress treatments, which suggests a complex regulatory network underlying each response.¹² However, bulk population measurements are limited in their ability to link gene regulation with cellular phenotypes such as growth rate because they lack single-cell resolution. In addition, due to cost and practicality, genome-wide gene expression data are typically recorded at only a few time points, meaning that temporal dynamics are not followed in any detail.^{13,14} A final limitation of bulk measurements is an inability to capture phenotypic heterogeneity, whereby individual cells display different responses in space and time.^{15–20}

An important alternative to bulk expression measurements is to use fluorescent reporter constructs that allow the gene expression in single cells to be followed. This approach has indicated the

importance of temporal order in the activation of different genes within a regulon, e.g., for the SOS response, antibiotic stress, flagellar synthesis, and metabolic pathways.^{8,9,16,18,21–24} Spatial cell-cell variability can also emerge due to variability in the concentrations of stress agents and metabolites in cell populations.^{15,17,25} The result can be complex spatiotemporal gene expression patterns under stress, which are shaped by cell-cell interactions, feedback between cell growth rate and gene expression,^{20,26,27} and environmental fluctuations.^{19,20,28,29} It is also becoming increasingly clear that stress survival is only partly determined by the protective responses of each individual cell but is strongly dependent on the collective protection provided by cell populations. However, to date, most single-cell studies have focused on one or a few reporter genes for a given stress or disregarded the potential for cellular interactions, which leaves open the question of how whole stress response regulons are coordinated in cell populations.

Here, we leverage the recent advancements in single-cell imaging that allow cellular behavior to be followed in a constantly controlled environment for long durations.^{18–20} We focus on the oxidative stress response of *Escherichia coli* to hydrogen peroxide (H₂O₂). H₂O₂ is a major reactive oxygen species that causes damage to proteins, lipids, and DNA. H₂O₂ readily permeates cells,²⁷ where it causes redox imbalance.³⁰ This stress leads to oxidation and a conformational change in the transcription factor OxyR.^{31,32} OxyR acts as a sensor for intracellular H₂O₂ levels and controls an array of more than two dozen genes in its regulon. OxyR-regulated genes are involved in diverse



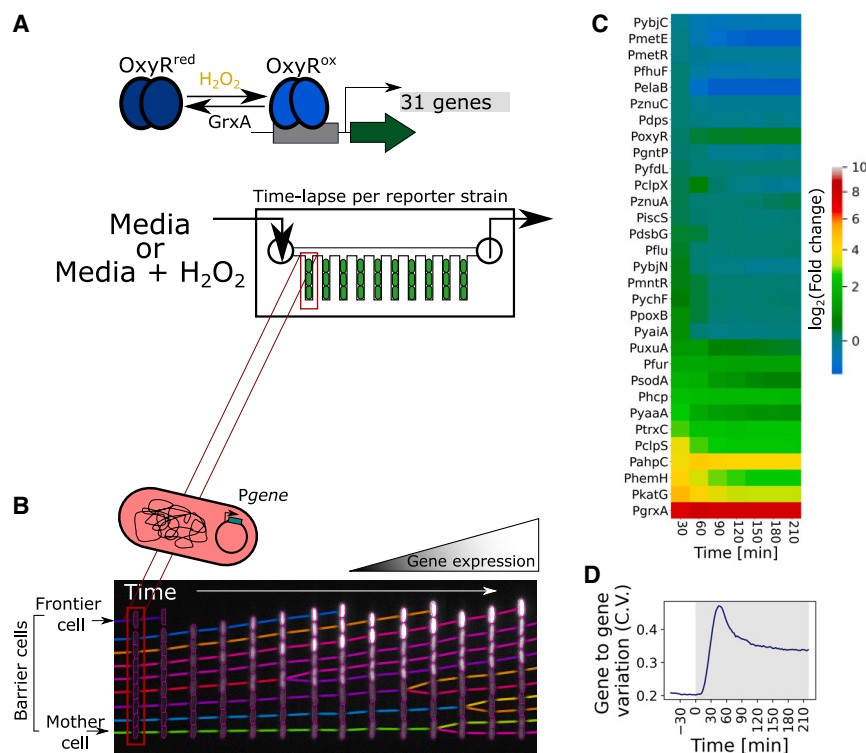


Figure 1. Gene expression dynamics across the OxyR regulon under H₂O₂ treatment

(A) Upon exposure to hydrogen peroxide, oxidation of OxyR leads to induction of a wide regulon of genes in *E. coli*. The schematic displays the microfluidics-based methodology to visualize the promoter activity of 31 fluorescently tagged transcriptional reporters by time-lapse microscopy at single-cell resolution.

(B) The kymograph represents cell growth over time in one of the representative growth channels, with intensity of cells reporting gene expression levels. We define “mother cells,” “barrier cells,” and frontier cells according to their position relative to the open end of the growth channel where growth media, with or without H₂O₂ treatment, is provided.

(C) Heatmap represents mean log₂-fold change in gene expression relative to basal level of frontier cells for 31 transcriptional reporters at 30-min intervals during continuous treatment with 100 μM H₂O₂ from t = 0 min (n ≥ 1,000 cells and ≥ 2 repeats per gene).

(D) Coefficient of variation (CV) for gene-to-gene expression variability across the 31 transcriptional reporters of frontier cells under 100 μM H₂O₂ treatment provided at t = 0 min. (Shaded region represents H₂O₂ treatment; n ≥ 1,000 cells and ≥ 2 repeats per gene.)

functions to maintain cell survival under H₂O₂ stress,^{4,33–36} including metal ion homeostasis,^{37–41} H₂O₂ scavenging,^{30,42,43} and redox maintenance.^{44–46} We combine experiments and theory to characterize and understand the transcriptional regulation of 31 genes, which have been previously identified as part of the oxidative stress response^{4,30,32,36–42,44–60} (Table S1). In this way, we are able to explain how a single transcription factor coordinates tens of genes in space and time to protect cells.

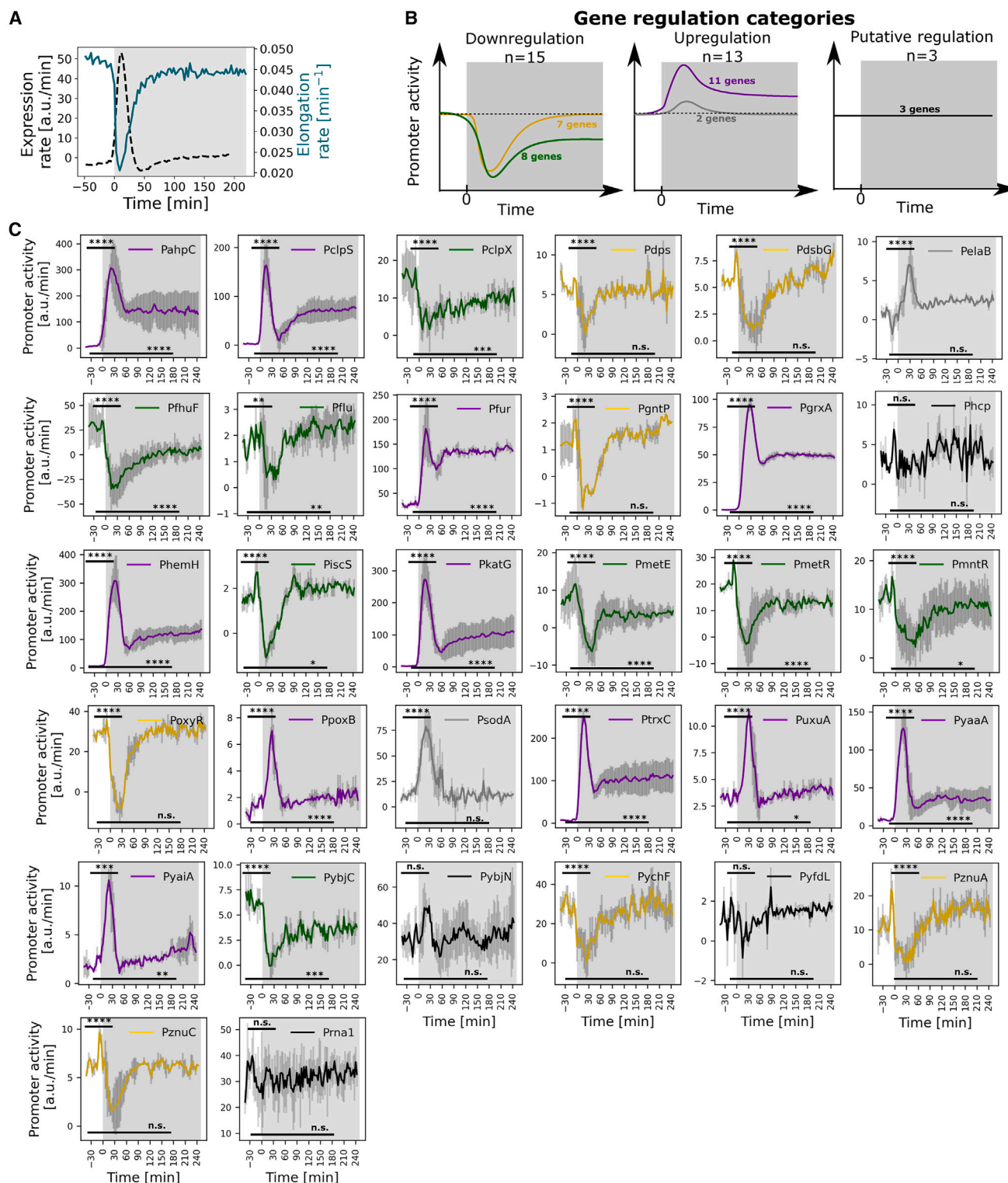
RESULTS

Genes in the OxyR regulon show variable responses to stress

We imaged gene expression dynamics using time-lapse microscopy of *E. coli* cells, each carrying one of 31 plasmid-based transcriptional reporters that have an OxyR-regulated promoter followed by a fast-maturing fluorescent protein (GFPmut2⁶¹ or sCFP3A for PkatG, PphpC, and PgrxA^{28,62}). Specifically, we chose promoters with OxyR binding sites according to chromatin immunoprecipitation measurements by Seo et al.^{36,63–67} and promoters that show changes in transcription according to RNA sequencing (RNA-seq) measurements by Roth et al.⁴ The resulting 31 promoters encompass the currently known OxyR regulon in *E. coli* (Table S1). We collected data for ~10,000 individual cells growing inside microfluidic growth trenches (“mother machine type”) during continuous H₂O₂ stress from ~2 h before until 6 h of treatment at 3-min time intervals, resulting in a rich dataset of ~200,000 expression measurements per reporter gene per hour (Figure 1A). The microfluidic chip provides an opportunity to disentangle genuine gene regulatory dynamics from envi-

ronmental changes because the continuous inflow of fresh media with H₂O₂ keeps the treatment concentration constant despite changes in the H₂O₂ scavenging capacities of cells. Unless stated otherwise, our analysis focused on the “frontier cells,” which are located at the open end of the growth trenches, where they are directly exposed to the H₂O₂ treatment from the media flow channel (Figure 1B). Due to efficient absorption and scavenging of H₂O₂, the cells located beneath the frontier cells experience diminishing concentrations of H₂O₂ and thus a lower stress response.²⁸ Another feature of our approach is to study the AB1157 strain of *E. coli* that carries an amber mutation in RpoS.⁶⁸ This allows us to isolate the role of OxyR in gene regulation without the influence of stationary phase regulation of certain oxidative stress response genes by RpoS.^{63,64,66}

With this setup, we were able to observe that all 31 genes showed an initial expression pulse within 30 min after the start of treatment (Figures 1C and S1), but expression of different genes diverged after this initial pulse. This variability fits with observations on the expression dynamics of the oxidative stress response of *Pseudomonas aeruginosa*.⁶⁹ After 90 min of continuous H₂O₂ treatment, most genes remained upregulated whereas others became downregulated relative to the untreated expression level (Figures 1C and S1). To further characterize differences in the regulation between genes, we computed the coefficient of variation (CV, variance normalized by the mean) across the expression levels of the 31 genes. The gene-to-gene variation was low in untreated cells, greatest during the transient expression peak shortly after treatment, and intermediate during steady state with continuous H₂O₂ treatment (Figure 1D). These patterns suggest that the genes vary not only in



(legend continued on next page)

expression magnitude but also show pronounced differences in induction timing and dynamics.

Transient growth inhibition causes a genome-wide expression pulse during stress

Our methodology enables us to analyze individual cell growth dynamics alongside gene expression. Importantly, this analysis revealed that the expression pulse at the start of H₂O₂ treatment precisely coincides with a period of transient growth inhibition (Figure 2A). During normal growth, protein concentrations stay constant in a cell on average because the expression rate is balanced with the dilution of molecules due to cell growth and division. H₂O₂ stress is known to rapidly stall cell growth, which is triggered by an OxyS-mediated cell-cycle arrest.⁷⁰ To remove the effect of growth dynamics on genes in the OxyR regulon, we normalized changes in expression level by the cell growth rate to give a measure of the promoter activity.¹⁶ Correcting for growth-rate effects revealed that 3 of the 31 genes (*Phcp*, *PyfdL*, and *PybjN*) showed no significant change in promoter activity at any time (Figures 2B and 2C; Videos S1 and S2). Moreover, another 9 of the genes (7 downregulated and 2 upregulated) showed only a transient change in regulation during the first ~100 min of treatment. These promoters return to baseline expression levels even though H₂O₂ is still present at a constant external concentration. Although most genes display consistent up- or downregulation throughout H₂O₂ treatment, a few genes show initial downregulation followed by upregulation at the steady state. For simplicity, we categorized the direction of regulation based on the changes in promoter activity immediately after treatment. Focusing our characterization on genes with lasting changes in promoter activity left 11 upregulated genes and 8 downregulated genes that showed a prolonged response to stress.

An interesting consequence of the effects of growth arrest on expression levels in the cell is that the genes that we identify as downregulated still show a positive pulse in expression levels after treatment (Figures 2B and 2C). In other words, the transcription rate from these promoters is downregulated in response to H₂O₂, but the reduction in growth rate outweighs this effect, resulting in an effective accumulation of proteins and the illusion of gene upregulation. These conclusions are supported by using the replication control promoter *Prna1* of plasmid PBR322 as a control, which is constitutively expressed and not part of the OxyR regulon.⁷¹ Our analysis shows that this promoter displays a similar expression pulse but maintains constant promoter activity in response to H₂O₂ treatment (Figures 2C and S1; Video S3). That is, we find that the growth-arrest-dependent accumulation of proteins is a global genome-wide effect and not specific to oxidative stress response genes.

Upregulated genes display either pulsatile or gradual dynamics

We next focused on the 11 genes whose gene expression changes and remains upregulated with H₂O₂ treatment

(Figures 2B and S2). Because we had found that gene-to-gene differences in expression were largest during the transient expression peak, we plotted the reporter expression level during the transient peak vs. the level at steady state (Figure 3A). This analysis reveals that the upregulated genes cluster on 2 distinct slopes. Seven of the upregulated genes (*PkatG*, *PyaaA*, *PclpS*, *PhemH*, *PuxuA*, *PpoxB*, and *PyaiA*) all have a high ratio of *peak/steady state* ~3, whereas the other upregulated genes (*PgrxA*, *PtrxC*, *Pfur*, and *PahpC*) share a lower ratio of *peak/steady state* ~1.5 (Figure 3B). The first class of genes showed a strong initial expression pulse that decays rapidly after its peak and stabilizes at a low steady-state level (hence termed “pulsatile”). In contrast, the second class of genes with a lower *peak/steady-state* ratio showed a gradual induction to an elevated steady-state level (hence termed “gradually responding”) (Figures 3C and 3D; Videos S1 and S2). After classifying the upregulated genes into two groups based on the *peak/steady state* ratio, we analyzed the mother cells located at the closed end of the growth trenches to follow the gene expression dynamics of the same cells for longer durations. We found that the pulsatile genes are generally activated earlier after the onset of H₂O₂ stress, achieving their maximal expression in 25.7 ± 4.7 min compared with 37.5 ± 7.8 min post H₂O₂ treatment for the non-pulsatile genes (Figures 3E and S2; Videos S1 and S2).

Modeling explains how differences in OxyR binding generate pulsatile or gradual dynamics

What explains the different patterns of upregulation? The oxidative stress response involves feedback from various metabolic pathways^{4,32,36,41,48,49,53–55} and several genes in the OxyR regulon are co-regulated by more than one transcription factor.^{36,63–67} Differences in the expression of genes in the OxyR regulon, therefore, may arise in multiple ways. However, we hypothesized that the differences we are seeing in the two classes of upregulated genes have a simpler underlying cause in the properties of OxyR itself. To explore this, we turned to a published mathematical model from our previous work, which uses coupled ordinary differential equations to describe changes in gene expression over time. Here, H₂O₂ permeates through the cell membrane and oxidizes OxyR, which leads to the induction of genes of the oxidative stress response regulon⁷² (Figure 4A). For simplicity, we reduced the operon to include only *grxA* (glutaredoxin-1) that converts OxyR back to its reduced form, the genes *ahpCF* (alkyl hydroperoxidase) and *katG* (catalase) that scavenge intracellular H₂O₂, and a “reporter gene” that is induced by OxyR but does not have a functional role (to mimic the fluorescent protein reporters used in experiments). Genes have a constant basal expression rate and their expression increases on induction by oxidized OxyR and decreases due to dilution by cell growth. The cell growth rate slows down with increasing H₂O₂ concentration, which in turn affects the protein dilution rate. The equations include constants for gene expression rates and enzyme efficiencies (Km and Kcat) that were obtained from literature or determined

(C) Mean promoter activity of frontier cells for 31 transcriptional reporters (ordered alphabetically) and the constitutively expressed promoter *Prna1-mKate2* with constant 100 μ M H₂O₂ treatment from $t = 0$ min (shaded region). Promoter activity shows the expression rate corrected for changes in cell growth rate. Non-parametric Mann-Whitney tests were used to indicate significant changes in promoter activity at the peak ($t = 9$ –60 min) or steady state ($t = 120$ –180 min) relative to the basal level expression ($t < 0$ min); where **** $p \leq 0.0001$, *** $p \leq 0.001$, ** $p \leq 0.01$, * $p \leq 0.05$, and n.s. (not significant) $p > 0.05$. Line colors correspond to the gene regulation categories as explained in (B). Error bars represent standard deviation ($n \geq 1,000$ cells and ≥ 2 repeats per gene).

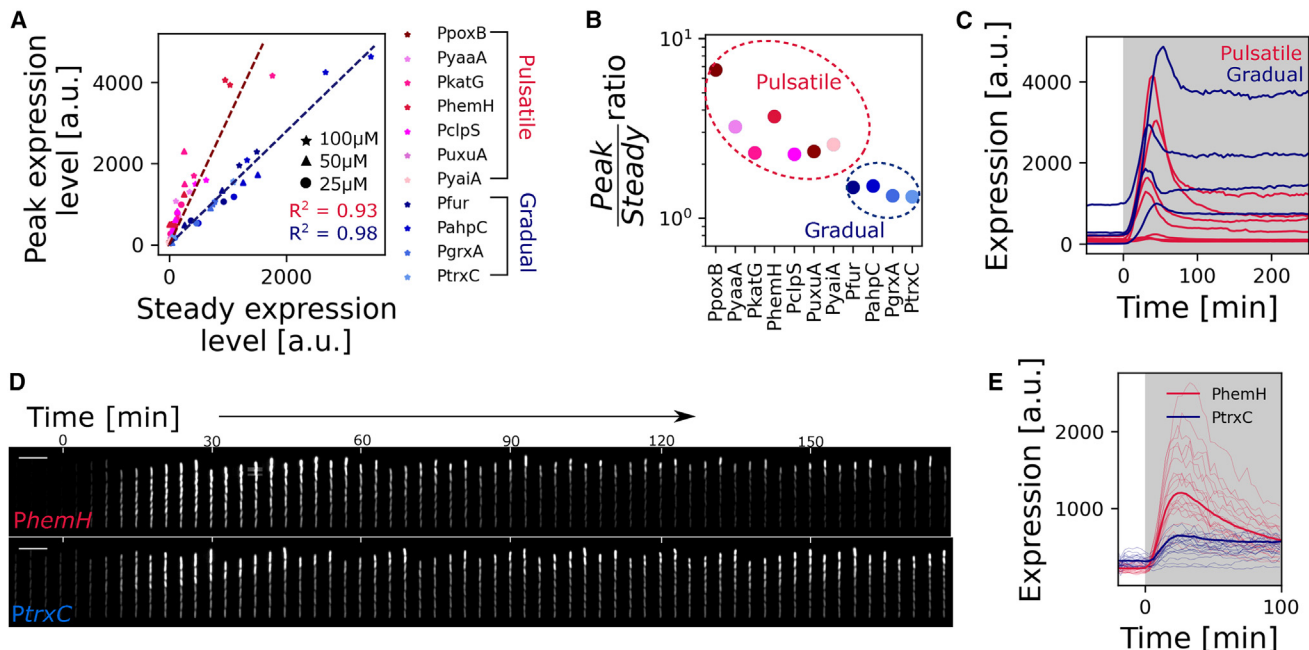


Figure 3. Upregulated promoters show either pulsatile or gradual induction dynamics

(A) Plot of the peak expression level (during the transient phase) vs. the expression level at steady state of frontier cells relative to basal expression for the indicated transcriptional reporters with 25 μM (circle), 50 μM (triangle), and 100 μM (star) H_2O_2 treatment. The pulsatile (pink) and gradually responding (blue) genes cluster on two distinct slopes, shown with linear fits (dashed lines).
(B) Peak/steady state ratio obtained by linear regression of values for individual genes shown in (A) cluster into two categories (pink, pulsatile genes; blue, gradually responding genes, $n \geq 3$ repeats per gene).
(C) Plot shows mean reporter expression levels of frontier cells for pulsatile (pink) and gradual (blue) genes under 100 μM H_2O_2 treatment provided at $t = 0$ min (shaded region) ($n \geq 1,500$ and $n \geq 3$ repeats per gene).
(D) Kymograph of *PhemH* and *PtrxC* transcription reporter expression representative of pulsatile and gradual induction with 100 μM H_2O_2 from $t = 0$ min, respectively (scale bar, 10 μm).
(E) Plot shows mean (bold) and single-cell (thin) reporter expression levels of mother cells for *PhemH* (pink, pulsatile) and *PtrxC* (blue, gradual) under 100 μM H_2O_2 treatment provided at $t = 0$ min (shaded region).

from previous experiments. The model was solved numerically to produce time-traces of gene expression levels.

We previously showed that this model recapitulates many aspects of the gene regulatory response and growth dynamics of *E. coli* with H_2O_2 treatment.⁷² Here, we employ the model to understand the basis for the different expression patterns seen across the genes in the OxyR regulon. We first tested the model's ability to explain the passive gene induction caused by the growth-arrest-dependent accumulation of proteins. As predicted, when the expression of the reporter gene was uncoupled from OxyR regulation in the model, it still showed the expression pulse during the transient growth arrest while the promoter activity stayed constant (Figure 4B). This mimics the behavior of the constitutive *P_{ma1}* promoter. In addition, for a reporter gene that is downregulated by OxyR, we again observe a similar induction pulse followed by a decrease in expression (Figure 4C).

To further explain the data, we extended the model to explicitly describe the effects of OxyR-dependent gene regulation based upon two parameters: K_{ind} captures the maximal expression rate when the promoter is fully occupied by oxidized OxyR and K_D captures the dissociation constant of oxidized OxyR from the promoter. Varying only these two parameters allowed us to shift expression dynamics in upregulated genes from gradual

to pulsatile, as observed in the data. Specifically, changing K_D affects the peak/steady-state ratio of the gene, with pulsatile genes being characterized by a high K_D value (Figure 4D). K_{ind} meanwhile determines the position of the gene along the slope in a peak vs. steady-state plot. Our model predicts, therefore, that the two categories of gene regulation, pulsatile and gradual, are the result of distinct promoter-dissociation constants of OxyR (Figures 4D–4F). In support of this, experiments by Tartaglia et al. showed that the dissociation constant of oxidized OxyR from the pulsatile gene promoter *P_{katG}* is an order of magnitude higher than for the *P_{ahpC}* promoter, which shows a gradual response⁷³ (Figure 4F). We conclude, therefore, that the divergent patterns in gene regulation in the regulon can be explained by coupling a simple OxyR redox switch with patterns of cell growth under stress. Furthermore, although other transcription factors are known to control some of the genes in the OxyR regulon,^{36,63–67} we found that OxyR alone was sufficient in our model for explaining the expression patterns seen under the conditions of our measurements (exponential growth with H_2O_2 treatment).

Pulsatile genes protect against sudden stress

What is the benefit of pulsatile expression of some genes and gradual induction of others? The model shows how the

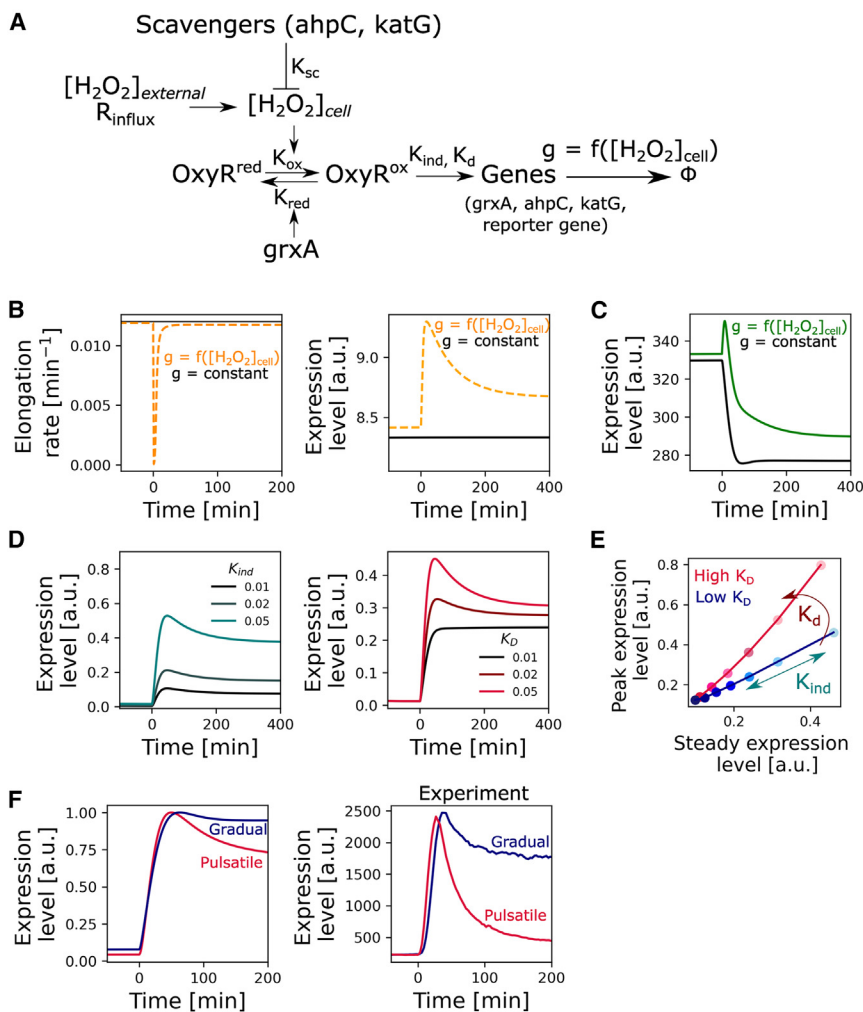


Figure 4. A model of the oxidative stress response predicts the molecular basis of the different categories of gene regulation

(A) Schematic represents the oxidative stress response model. The cells experience influx of H_2O_2 at R_{influx} rate, causing OxyR oxidation and induction of stress response genes. GrxA (glutaredoxin-1) converts oxidized OxyR back to its reduced form and scavenging enzymes encoded by *ahpCF* and *katG* lower the intracellular $[H_2O_2]_{\text{cell}}$ concentration. The expression of the proteins is balanced by dilution due to cell growth, where the cell elongation rate g is a function of $[H_2O_2]_{\text{cell}}$. OxyR also regulates a reporter gene that has no function in the response itself.

(B) Effect of growth inhibition by H_2O_2 on gene expression dynamics. (Left) Cell elongation rate affected by intracellular H_2O_2 concentration (orange, dashed) compared with constant elongation rate unaffected by H_2O_2 treatment provided at $t = 0$ min. (Right) Expression level of a constitutively expressed reporter gene (not regulated by OxyR) shows a passive induction pulse in the case where H_2O_2 inhibits cell elongation (orange) and no induction effect when the elongation rate is unaffected by H_2O_2 (black) treatment from $t = 0$ min.

(C) Expression dynamics of a downregulated reporter gene in the case where cell elongation rate is affected (green) or unaffected (black) by H_2O_2 .

(D) Induction of upregulated reporter genes for varying values of induction rate (K_{ind} , left) and promoter-dissociation constant of oxidized OxyR (K_D , right) with H_2O_2 treatment from $t = 0$ min. K_{ind}/K_D ratio was kept constant for curves with varying K_D .

(E) The plot shows the effect of K_{ind} (by treating cells with increasing concentrations of H_2O_2 - dark to light shade) and K_D (high = 0.1 a.u. and low = 0.01 a.u.) on the gene expression dynamics. Pulsatile genes with high peak/steady ratio are characterized by a higher K_D value, whereas K_{ind} determines the overall magnitude of the induction without affecting the peak/steady ratio.

(F) Mean gene expression levels from model (left) and experiments (right) of representative genes for the two categories of upregulation—*PkatG* (pink, pulsatile gene) and *PahpC* (blue, gradually responding gene) of frontier cells treated with 100 μM treatment from $t = 0$ min ($n \geq 3$ repeats).

dissociation constant of OxyR affects sensitivity of genes to changes in H_2O_2 concentration. Specifically, promoters with a high K_D for OxyR show an approximately proportional increase in activity with H_2O_2 concentration, whereas the activity of promoters with a low K_D is less sensitive to H_2O_2 (Figure 5A). In support of this prediction, experiments show that rising H_2O_2 concentration causes a much steeper increase for the pulsatile *PkatG* promoter activity compared with the *PgrxA* promoter, which shows a gradual response (Figures 5A and S3). Similarly, other pulsatile genes showed a higher sensitivity to H_2O_2 compared with gradually responding genes (Figures 5B and S3). In *Mycobacterium tuberculosis*, induction of *katG* showed higher sensitivity for H_2O_2 than *ahpC*,⁷⁴ matching the pulsatile behavior of *katG* and gradual induction of *ahpC* in *E. coli*. The model further predicts that the pulsatile gene induction is a consequence of a response to a transient spike in intracellular H_2O_2 , which accumulates until the increased level of scavenging enzymes tips the balance (Figure 5C). In support of this explanation, experiments show that the expression pulse of *PkatG* is

much reduced when cells respond to a graded increase in the dose of H_2O_2 as opposed to a step treatment (Figure 5D).

These analyses suggest that pulsatile genes are important in response to sudden stress, whereas gradually responding genes are more important during prolonged stress. Consistent with this hypothesis, deletion of the pulsatile *katG* gene makes cells extremely sensitive to sudden H_2O_2 treatment, leading to complete growth arrest and inability to induce the oxidative stress response (Figures 5E and 5F; Video S4). However, ΔkatG cells were still able to survive and adapt to a graded increase in the dose of H_2O_2 , reaching the same final concentration (Figure 5F). That is, the expression pulse of *katG* appears to be critical for the rapid production of catalase enzymes to counteract the transient spike in intracellular H_2O_2 , but *katG* expression becomes dispensable after the initial adaptation delay, as noted before.⁶² H_2O_2 tolerance during prolonged exposure is then provided by the gradually responding AhpCF alkyl hydroperoxidase, which scavenges lower concentrations of H_2O_2 efficiently.³⁰

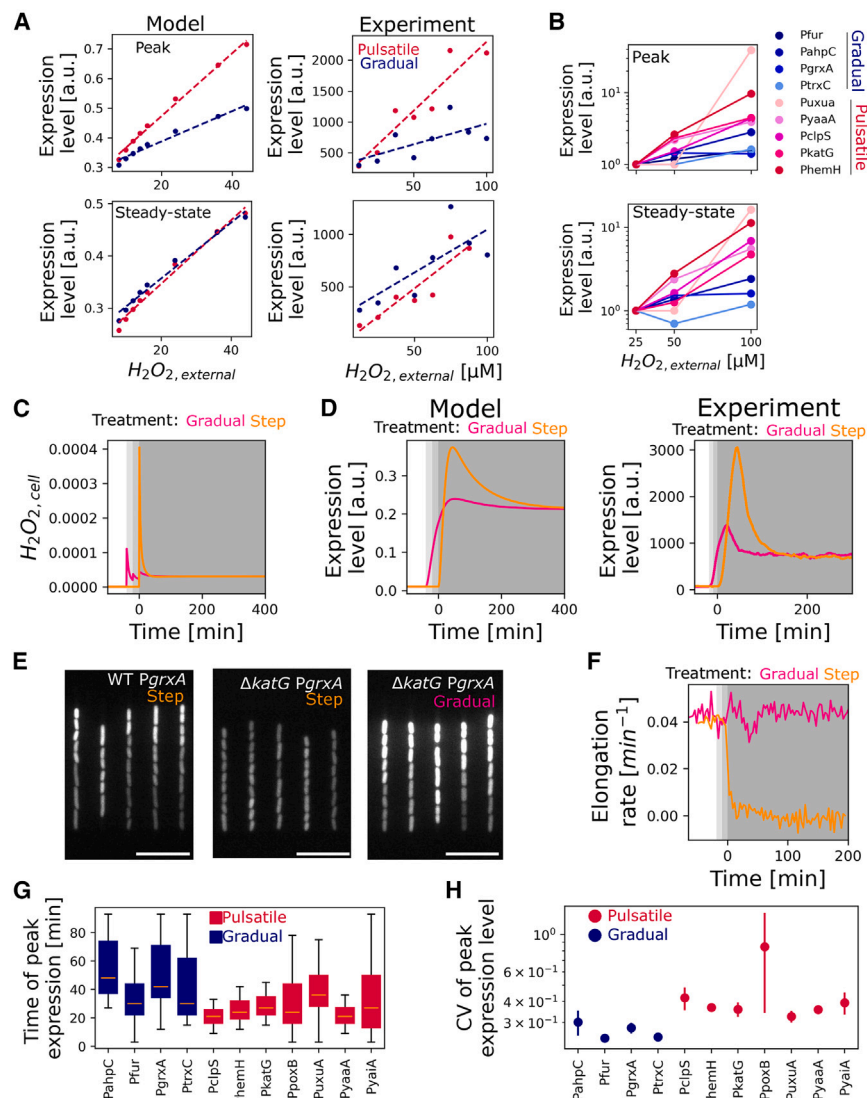


Figure 5. Pulsatile genes respond quickly to bridge the adaptation lag after H_2O_2 treatment

(A) The response of pulsatile genes (high K_D) is more sensitive to changes in H_2O_2 concentration than gradually responding genes (low K_D). Model outputs (left) and experimental data (right) for expression level at peak (top) and steady state (bottom) of *PkatG* (pulsatile gene, pink) and *PgrxA* (gradually responding, blue) across a range of external H_2O_2 concentrations. Dashed lines show linear fits.

(B) Relative changes in gene expression at peak (top) and steady state (bottom) of frontier cells with H_2O_2 treatment ranging from 25 to 100 μM H_2O_2 . Pulsatile genes (pink) show higher dose-sensitivity compared with gradually responding genes (blue) ($n \geq 2$ repeats per gene per H_2O_2 concentration).

(C) Model results of intracellular $H_2O_{2,cell}$ concentration with step treatment (100 units H_2O_2 , orange) from $t = 0$ min or graded increasing doses of H_2O_2 treatment (from 25 to 50 to 100 units H_2O_2 , pink).

(D) Mean expression levels for model (left) and experiments (right) of pulsatile gene *PkatG* for step (100 μM H_2O_2 , orange) or graded increasing doses of H_2O_2 treatment (from 25 to 50 to 100 μM H_2O_2 , pink) as depicted in (C) ($n \geq 2$ repeats).

(E) Snapshot of *PgrxA* expression at steady state for step treatment (left and middle) or graded increasing doses of H_2O_2 treatment (right, as shown in C and D) for wild-type (left) cells and $\Delta katG$ cells (middle and right) after 120 min of treatment with 100 μM H_2O_2 (scale bar, 10 μm).

(F) Graded increasing doses of H_2O_2 treatment enable adaptation of $\Delta katG$ cells. Mean elongation rate for $\Delta katG$ cells (located at a position with 3 barrier cells) treated with 100 μM H_2O_2 in a step (orange) or graded (pink) manner (as depicted in C–E, $n \geq 2$ repeats).

(G) Boxplots indicate the median of time taken to reach the peak gene expression for individual mother cells under 100 μM H_2O_2 step treatment (gradually responding genes: blue, pulsatile genes: pink; box length extends to the lower and upper

quartile with error bars representing the range, $n \geq 3$ repeats per gene).

(H) Mean coefficient of variation (CV) for peak gene expression values of frontier cells showing cell-to-cell heterogeneity under 100 μM H_2O_2 step treatment (blue: gradually responding genes, pink: pulsatile genes, error bars represent standard deviation, $n \geq 3$ repeats per gene).

Pulsatile genes show higher cell-to-cell expression heterogeneity

We next asked to what extent the expression of pulsatile and gradually responding genes is coordinated within the same cell. For this, we followed the expression dynamics of mother cells (which can be monitored in the channels for many generations) and found that the time of induction after the onset of stress was shorter and less variable across cells for the pulsatile genes (Figure 5G). However, the amplitude of the expression peak reached by individual cells was more variable for pulsatile genes compared with gradually responding genes (Figures 5H, S1, and S4). Regulation of pulsatile genes, therefore, appears to prioritize precise control of the timing over the magnitude of the response (Figures 5G, 5H, and S4). That is, this form of regulation functions to activate a response very quickly, if not accurately, in the face of rapid onset stress.

Next, we constructed a dual-reporter strain with two fluorescently labeled transcriptional reporters: the pulsatile *PkatG*-YFP (yellow fluorescent protein) reporter expressed from a plasmid and the gradually responding *PgrxA*-CFP (cyan fluorescent protein) reporter inserted on the chromosome (Figure 6A; Video S5). We also constructed a control strain with two *PgrxA* reporters, one marked with CFP on the chromosome and one marked with YFP on the plasmid, to account for variability due to differences in fluorescent proteins (YFP vs. CFP) and the difference in gene copy numbers of the reporters (chromosomal vs. multi-copy plasmid) (Figure 6A; Video S6). The mean expression dynamics of the dual-reporter strains matched our previous analysis for *PkatG* and *PgrxA* in single reporter strains (Figure 6B; Video S5). Interestingly, for the control strain, the plasmid-expressed *PgrxA* displayed a slightly higher expression pulse compared

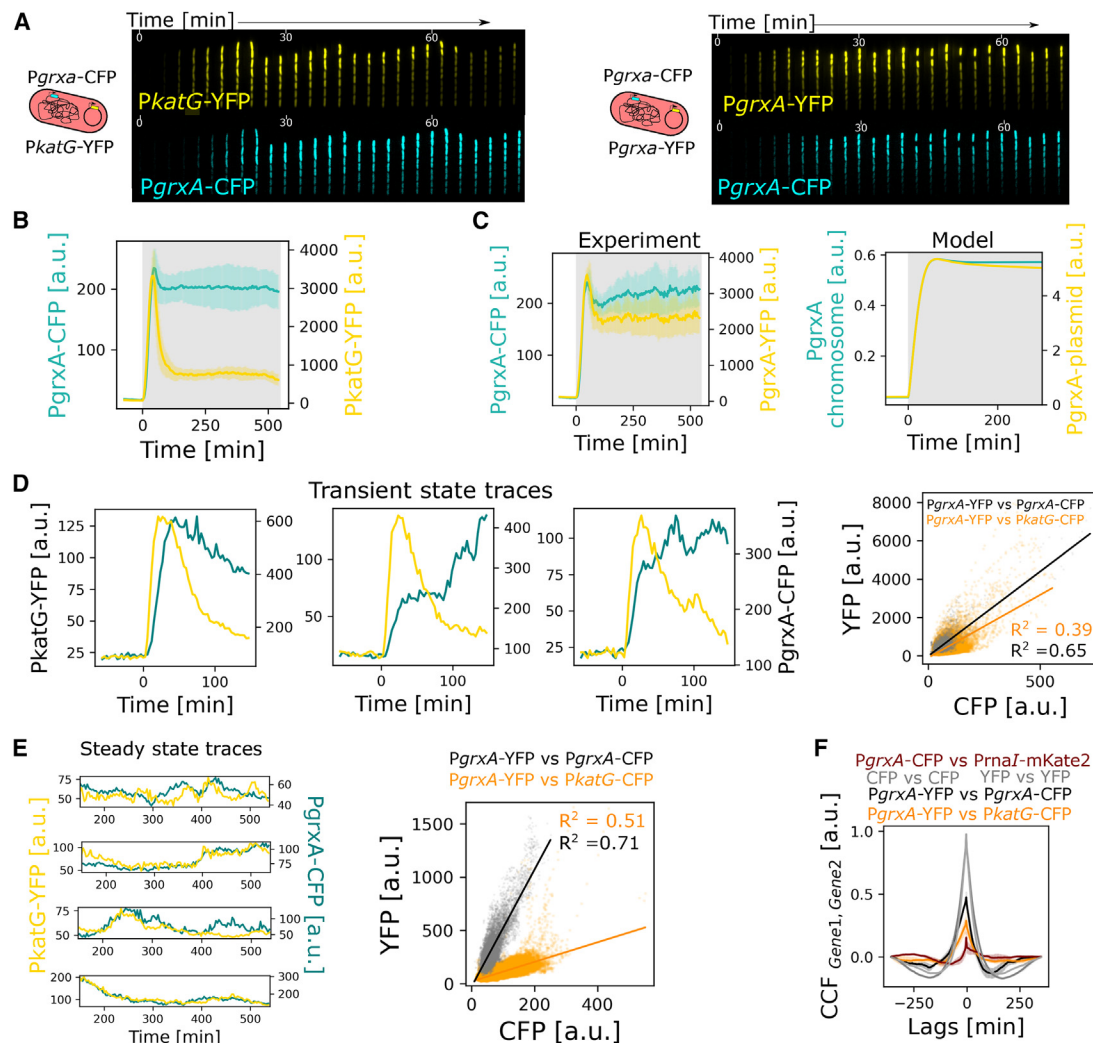


Figure 6. Coordination of pulsatile and gradual gene regulation in single cells

(A) *E. coli* dual-reporter strains with *PkatG*-YFP on plasmid + *PgrxA*-CFP on chromosome (left) and *PgrxA*-YFP on plasmid + *PgrxA*-CFP on chromosome (right, control strain). Kymographs represent gene expression levels for both reporters in cells treated with 100 μ M H_2O_2 at $t = 0$ min.

(B) Mean expression of *PgrxA*-CFP (cyan) and *PkatG*-YFP (yellow) for frontier cells under 100 μ M H_2O_2 provided at $t = 0$ min ($n = 3$ repeats, error bars: standard deviation).

(C) Mean expression of *PgrxA*-CFP (cyan) and *PgrxA*-YFP (yellow) for frontier cells under 100 μ M H_2O_2 provided at $t = 0$ min from experiments (left) and model output (right) ($n = 3$ repeat, error bars: standard deviation).

(D) (Left) Representative expression of *PkatG*-YFP (yellow) and *PgrxA*-CFP (cyan) for individual mother cells after treatment with 100 μ M H_2O_2 from $t = 0$ min. (Right) Peak expression of *PgrxA*-YFP vs. *PgrxA*-CFP (black) and *PgrxA*-YFP vs. *PkatG*-CFP (orange) for mother cells after treatment with 100 μ M H_2O_2 . The lines represent linear fits.

(E) (Left) Representative expression traces of *PkatG*-YFP (yellow) and *PgrxA*-CFP (teal) for individual mother cells during steady state with 100 μ M H_2O_2 treatment from $t = 0$ min. (Right) *PgrxA*-YFP vs. *PgrxA*-CFP (black) and *PgrxA*-YFP vs. *PkatG*-CFP (orange) expression for mother cells during steady state with 100 μ M H_2O_2 treatment. The lines represent the linear regression fit to the datasets. R^2 : Pearson correlation coefficient.

(F) Mean temporal cross-correlation of steady-state expression dynamics between *PgrxA*-YFP and *PgrxA*-CFP (black), *PgrxA*-YFP and *PgrxA*-CFP (gray), *PgrxA*-YFP and *PkatG*-CFP (orange) for mother cells under 100 μ M H_2O_2 treatment.

with the *PgrxA* reporter on the chromosome, even after normalizing for differences in the steady-state level (Figure 6C). This is a subtle but significant effect and explained by our model, which showed that the plasmid copy number increases transiently when the cell growth rate slows during the onset of H_2O_2 treatment (Figure 6C). This effective increase in gene dosage leads to an additional expression boost for the plasmid-based promoter.

Focusing on the dual-reporter strain, we found that *PkatG* and *PgrxA* expression in the same mother cell showed relatively little correlation during the transient expression pulse (Figure 6D; Video S5). However, both promoters exhibited substantial fluctuations in gene expression during prolonged treatment, and we found that these fluctuations were closely correlated (Figure 6E; Video S5). This was evident from gene expression levels at discrete time points and from temporal cross-correlation

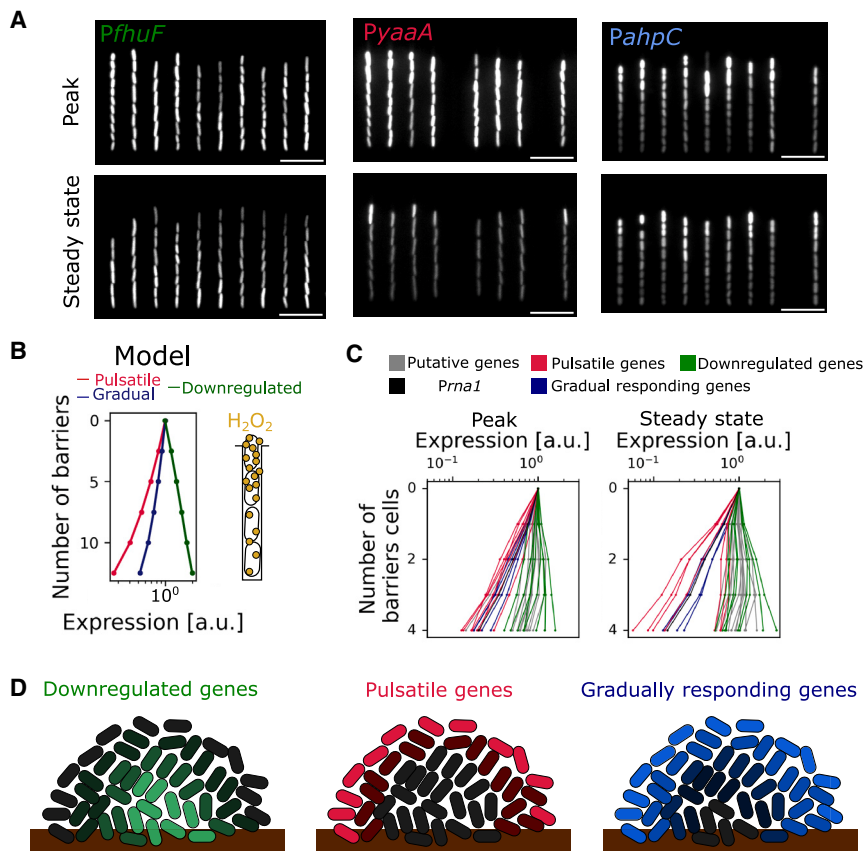


Figure 7. Spatiotemporal expression patterns across the OxyR regulon

(A) Snapshots of cells with representative reporters for the three categories of gene regulation: *Pfhuf* (downregulated), *PyaaA* (pulsatile), and *PahpC* (gradually responding) during peak expression (top) and at steady state (bottom) with 100 μM H_2O_2 treatment.

(B) Scavenging of H_2O_2 by bacteria creates $\text{H}_2\text{O}_{2\text{external}}$ gradients in the growth trench from the source of treatment at the open end to the mother cell at the closed end. Model output for the expression of pulsatile (KatG, pink), gradually responding (GrxA, blue), and downregulated (negatively regulated reporter, green) genes for cells across the growth trench (increasing number of barrier cells) relative to the expression of frontier cells. Schematic illustrates gradient in $\text{H}_2\text{O}_{2\text{external}}$ along the growth trench.

(C) Mean expression of 31 transcriptional reporters for cells with different numbers of barrier cells with 100 μM H_2O_2 treatment relative to the expression of frontier cells during peak expression (left) and steady state (right) (pulsatile: pink, gradual: blue, down: green, constitutive *Prra1-mKate2*: black, putative: gray; $n \geq 3$ repeats per gene).

(D) Schematic depicting the expected spatial variation across a bacterial population in the expression of OxyR-controlled genes that are downregulated (green, left), pulsatile induced (red, center), and gradually responding (blue, right) under H_2O_2 treatment.

analysis (Figure 6F). Together, our single-cell analysis revealed that pulsatile and gradually responding genes are tightly coordinated during prolonged stress but appear to be uncoupled in regulation during the transient response to sudden stress.

Differentially regulated genes show distinct spatial patterns in cell populations

Spatial patterns of gene expression are important in the oxidative stress response because of the ability of cells nearest the stress to protect cells that are further away. This phenomenon is remarkably effective, with each individual cell reducing the local H_2O_2 concentration by around 30% in its vicinity inside the one-dimensional microfluidic channel.²⁶ Within colonies, cells are protected in all three dimensions by surrounding cells leading to even steeper spatial H_2O_2 gradients from the edge to the interior of the population.²⁸ However, how this spatial structuring affects the whole oxidative stress regulon is unknown. We, therefore, asked whether the different temporal expression patterns we observe across the regulon were associated with different spatial expression patterns.

Quantifying expression levels in the channels of the microfluidic device revealed clear differences in the spatial patterning of regulation across genes. Downregulated genes exhibited an inverse gradient to that of the stress, with the lowest expression seen in the frontier cells that are closest to the H_2O_2 source (Figures 7A and 7C; Video S2). Even passively induced genes that are not part of the OxyR regulon showed a spatial gradient in expression level that was driven by a more pronounced inhibi-

tion of growth for cells that are located closer to the H_2O_2 source (Figure 7C). Turning to upregulated genes, we see a steeper decay in expression in space as one moves away from the source of stress for pulsatile genes, as compared with the gradually responding genes, in both our model and experiments (Figure 7; Video S1). That is, pulsatile genes are strongly upregulated in relatively few cells that are close to the H_2O_2 source, which generates significant cross-protection, such that only the most stressed cells show expression. Conversely, downregulated genes are more strongly expressed in the interior of a population. The gradually upregulated genes then activate more evenly in larger numbers of cells to provide lasting protection. Figure 7D illustrates the resulting pattern of gene expression in a cell colony.

DISCUSSION

The rapid and coordinated regulation of stress response genes is critical for survival in a changing environment.⁷⁵ However, bulk measurements provide limited insights into how gene expression dynamics are coordinated in space and time within cell populations. To address this, we leveraged the power of single-cell transcriptional reporters to follow the bacterial oxidative stress response under continuous H_2O_2 treatment. Our work revealed a diverse set of dynamics across 31 oxidative stress response genes. Despite this diversity, our modeling and experiments show that OxyR binding dynamics together with the effects of stress on the cell growth rate can explain the different gene regulation patterns. Promoters with a negative K_{ind} exhibit reduced

expression rate, despite the fact that protein levels transiently increase due to a slowdown of cell growth. For upregulated genes, promoters with a high K_D drive a strong transient expression pulse after H_2O_2 treatment, leading to pulsatile expression, whereas promoters with a lower K_D activate genes more slowly and sustain elevated expression rates throughout prolonged treatment. Moreover, by using a dual reporter, we show that the expression of different genes in the stress response diverges during the initial rapid response to treatment but then becomes closely correlated at steady state.

The dynamics we observe are broadly consistent with previous bulk measurements^{4,36,49} for time points shortly after the start of treatment (Table S1). We observe differences at later time points (Figure S5). However, these differences are to be expected because bulk methods typically study gene expression in dense cultures after a single high dose of H_2O_2 . H_2O_2 levels decay quickly in bulk cultures and the stress response abates, which is not the case with continuous supply of H_2O_2 in microfluidic chips.^{4,37,50} Although the microfluidics chips therefore provide clear advantages for this study, they do not fully reflect the conditions in larger cell populations. To address this, we previously conducted experiments on cell colonies and found that H_2O_2 treatment of colonies generated similar spatial gradients in stress responses as in microfluidic channels.²⁸ We also showed how the response gradients scale with increasing numbers of cells, both in microfluidic channels and in colonies⁷², meaning that results from microfluidics can be meaningfully extrapolated to larger cell populations.

What is the evolutionary function of the different patterns in gene regulation that we observe? Our model and experiments suggest that the higher H_2O_2 sensitivity of pulsatile genes provides a rapid defense against sudden bursts of intracellular H_2O_2 . Interestingly, several of the pulsatile genes, including *yaaA*,³⁸ *clpS*,³⁷ and *hemH*,⁴¹ are involved in iron regulation. Their pulsatile induction is likely beneficial to counter the rapid lethality of H_2O_2 experienced due to the Fenton reaction.^{62,76–79} Being more sensitive to local H_2O_2 fluctuations, pulsatile genes therefore display high cell-cell variability in expression magnitude and steeper spatial gradients compared with gradually responding genes. Of the two H_2O_2 scavenging enzymes, pulsatile catalase (*katG*) is important to protect against immediate stress experienced by cells on the periphery of a population, whereas gradually responding alkyl hydroperoxidase (*ahpCF*) efficiently scavenges low H_2O_2 levels that reach the rest of the population. Gradually responding thioredoxins (*grxA*⁷⁹ and *trxC*⁴⁶) regulate the redox status of proteins, including OxyR. In contrast to the pulsatile genes, the gradually responding genes show a more consistent response both in space and time, with more cells contributing to protection at the steady state. In this way, the action of a single transcription factor is able to orchestrate the stress response to generate both individual and collective protection.

RESOURCE AVAILABILITY

Lead contact

Further information and requests for resources and reagents should be directed to and will be fulfilled by Stephan Uphoff (stephan.uphoff@bioch.ox.ac.uk).

Materials availability

This study did not generate new materials.

Data and code availability

- All the raw data collected for analysis in this study have been deposited at the Oxford Research Archive (<https://ora.ox.ac.uk/objects/uid:1b2c7733-9fc2-475e-bd15-e4bf1cdc3e39>) and are publicly available as of the date of publication. DOIs are listed in the [key resources table](#).
- This paper does not report original code.
- Any additional information required to reanalyze the data reported in this paper is available from the [lead contact](#) upon request.

ACKNOWLEDGMENTS

We thank Somenath Bakshi, Georgia Isom, and members of the Uphoff and Foster labs for their discussions and comments on the manuscript. This study was supported by Wellcome Trust and Royal Society Sir Henry Dale Fellowship 206159/Z/17/Z (S.U.), Wellcome-Beit Prize 206159/Z/17/B (S.U.), Research Prize Fellowship of the Lister Institute of Preventative Medicine (S.U.), Oxford-Indira Gandhi Scholarship funded by the Oxford India Center for Sustainable Development (D.C.), European Research Council grant 787932 (K.R.F.), and Wellcome Trust Investigator award 209397/Z/17/Z (K.R.F.).

AUTHOR CONTRIBUTIONS

Conceptualization and design of study: D.C., K.R.F., and S.U.; data collection: D.C.; development of the computational model: D.C. and S.U.; data analysis and interpretation: D.C., K.R.F., and S.U.; writing of the article: D.C., K.R.F., and S.U.; supervision: K.R.F. and S.U.

DECLARATION OF INTERESTS

The authors declare no competing interests.

STAR★METHODS

Detailed methods are provided in the online version of this paper and include the following:

- [KEY RESOURCES TABLE](#)
- [EXPERIMENTAL MODEL](#)
 - Strains and plasmids
 - Media and growth conditions
- [METHOD DETAILS](#)
 - Microfluidic chip preparation and setup
 - Time-lapse microscopy
- [QUANTIFICATION AND STATISTICAL ANALYSIS](#)
 - Mother machine data processing and analysis
 - Linear regression analysis
 - Oxidative stress response model

SUPPLEMENTAL INFORMATION

Supplemental information can be found online at <https://doi.org/10.1016/j.cels.2024.10.003>.

Received: March 7, 2024

Revised: July 10, 2024

Accepted: October 21, 2024

Published: November 13, 2024

REFERENCES

1. Perez, J.C., and Groisman, E.A. (2009). Evolution of transcriptional regulatory circuits in bacteria. *Cell* 138, 233–244. <https://doi.org/10.1016/j.CELL.2009.07.002>.

2. Sanchez-Vazquez, P., Dewey, C.N., Kitten, N., Ross, W., and Gourse, R.L. (2019). Genome-wide effects on *Escherichia coli* transcription from ppGpp binding to its two sites on RNA polymerase. *Proc. Natl. Acad. Sci. USA* **116**, 8310–8319. https://doi.org/10.1073/PNAS.1819682116/SUPPL_FILE/PNAS.1819682116.SD02.PDF.
3. Durfee, T., Hansen, A.M., Zhi, H., Blattner, F.R., and Jin, D.J. (2008). Transcription Profiling of the Stringent Response in *Escherichia coli*. *J. Bacteriol.* **190**, 1084–1096. <https://doi.org/10.1128/JB.01092-07>.
4. Roth, M., Jaquet, V., Lemeille, S., Bonetti, E.J., Cambet, Y., François, P., and Krause, K.H. (2022). Transcriptomic Analysis of *E. coli* after Exposure to a Sublethal Concentration of Hydrogen Peroxide Revealed a Coordinated Up-Regulation of the Cysteine Biosynthesis Pathway. *Antioxidants (Basel)* **11**, 655. <https://doi.org/10.3390/ANTIOX11040655>.
5. Gunasekera, T.S., Csonka, L.N., and Paliy, O. (2008). Genome-Wide Transcriptional Responses of *Escherichia coli* K-12 to Continuous Osmotic and Heat Stresses. *J. Bacteriol.* **190**, 3712–3720. <https://doi.org/10.1128/JB.01990-07>.
6. Li, Y., Zhou, D., Hu, S., Xiao, X., Yu, Y., and Li, X. (2018). Transcriptomic analysis by RNA-seq of *Escherichia coli* O157:H7 response to prolonged cold stress. *LWT* **97**, 17–24. <https://doi.org/10.1016/J.LWT.2018.06.025>.
7. Tucker, D.L., Tucker, N., and Conway, T. (2002). Gene Expression Profiling of the pH Response in *Escherichia coli*. *J. Bacteriol.* **184**, 6551–6558. <https://doi.org/10.1128/JB.184.23.6551-6558.2002>.
8. Courcelle, J., Khodursky, A., Peter, B., Brown, P.O., and Hanawalt, P.C. (2001). Comparative gene expression profiles following UV exposure in wild-type and SOS-deficient *Escherichia coli*. *Genetics* **158**, 41–64. <https://doi.org/10.1093/GENETICS/158.1.41>.
9. Culyba, M.J., Kubiak, J.M., Mo, C.Y., Goulian, M., and Kohli, R.M. (2018). Non-equilibrium repressor binding kinetics link DNA damage dose to transcriptional timing within the SOS gene network. *PLoS Genet.* **14**, e1007405. <https://doi.org/10.1371/JOURNAL.PGEN.1007405>.
10. Wolfram-Schauerte, M., Pozhydaieva, N., Viering, M., Glatzer, T., and Höfer, K. (2022). Integrated Omics Reveal Time-Resolved Insights into T4 Phage Infection of *E. coli* on Proteome and Transcriptome Levels. *Viruses* **14**, 2502. <https://doi.org/10.3390/V14112502>.
11. Ma, P., Amemiya, H.M., He, L.L., Gandhi, S.J., Nicol, R., Bhattacharyya, R.P., Smillie, C.S., and Hung, D.T. (2023). Bacterial droplet-based single-cell RNA-seq reveals antibiotic-associated heterogeneous cellular states. *Cell* **186**, 877–891. <https://doi.org/10.1016/J.CELL.2023.01.002>.
12. Bhatia, R.P., Kirit, H.A., Predeus, A.V., and Bollback, J.P. (2022). Transcriptomic profiling of *Escherichia coli* K-12 in response to a compendium of stressors. *Sci. Rep.* **12**, 8788. <https://doi.org/10.1038/s41598-022-12463-3>.
13. Stanford, B.C.M., Clake, D.J., Morris, M.R.J., and Rogers, S.M. (2020). The power and limitations of gene expression pathway analyses toward predicting population response to environmental stressors. *Evol. Appl.* **13**, 1166–1182. <https://doi.org/10.1111/EVA.12935>.
14. Bervoets, I., and Charlier, D. (2019). Diversity, versatility and complexity of bacterial gene regulation mechanisms: opportunities and drawbacks for applications in synthetic biology. *FEMS Microbiol. Rev.* **43**, 304–339. <https://doi.org/10.1093/FEMSRE/FUZ001>.
15. Wang, T., Shen, P., He, Y., Zhang, Y., and Liu, J. (2023). Spatial transcriptome uncovers rich coordination of metabolism in *E. coli* K12 biofilm. *Nat. Chem. Biol.* **19**, 940–950. <https://doi.org/10.1038/s41589-023-01282-w>.
16. Kim, J.M., Garcia-Alcala, M., Balleza, E., and Cluzel, P. (2020). Stochastic transcriptional pulses orchestrate flagellar biosynthesis in *Escherichia coli*. *Sci. Adv.* **6**, eaax0947. <https://doi.org/10.1126/SCIADV.AAX0947>.
17. Serra, D.O., and Hengge, R. (2014). Stress responses go three dimensional – the spatial order of physiological differentiation in bacterial macro-colony biofilms. *Environ. Microbiol.* **16**, 1455–1471. <https://doi.org/10.1111/1462-2920.12483>.
18. Mitosch, K., Rieckh, G., and Bollenbach, T. (2019). Temporal order and precision of complex stress responses in individual bacteria. *Mol. Syst. Biol.* **15**, e8470. <https://doi.org/10.15252/MSB.20188470>.
19. Alnahhas, R.N., and Dunlop, M.J. (2023). Advances in linking single-cell bacterial stress response to population-level survival. *Curr. Opin. Biotechnol.* **79**, 102885. <https://doi.org/10.1016/J.COPBIO.2022.102885>.
20. Sampaio, N.M.V., Blassick, C.M., Andreani, V., Lugagne, J.B., and Dunlop, M.J. (2022). Dynamic gene expression and growth underlie cell-to-cell heterogeneity in *Escherichia coli* stress response. *Proc. Natl. Acad. Sci. USA* **119**, e2115032119. https://doi.org/10.1073/PNAS.2115032119/SUPPL_FILE/PNAS.2115032119.SM05.MP4.
21. Gasch, A.P., Spellman, P.T., Kao, C.M., Carmel-Harel, O., Eisen, M.B., Storz, G., Botstein, D., and Brown, P.O. (2000). Genomic expression programs in the response of yeast cells to environmental changes. *Mol. Biol. Cell* **11**, 4241–4257. <https://doi.org/10.1091/MBC.11.12.4241/ASSET/IMAGES/LARGE/MK1201389008.JPEG>.
22. Mitosch, K., Rieckh, G., and Bollenbach, T. (2017). Noisy Response to Antibiotic Stress Predicts Subsequent Single-Cell Survival in an Acidic Environment. *Cell Syst.* **4**, 393–403.e5. <https://doi.org/10.1016/J.CELS.2017.03.001>.
23. Alon, U. (2007). Network motifs: theory and experimental approaches. *Nat. Rev. Genet.* **8**, 450–461. <https://doi.org/10.1038/nrg2102>.
24. Zaslaver, A., Mayo, A.E., Rosenberg, R., Bashkin, P., Sberro, H., Tsalyuk, M., Surette, M.G., and Alon, U. (2004). Just-in-time transcription program in metabolic pathways. *Nat. Genet.* **36**, 486–491. <https://doi.org/10.1038/ng1348>.
25. Zoheir, A.E., Sobol, M.S., Meisch, L., Ordoñez-Rueda, D., Kaster, A.K., Niemeyer, C.M., and Rabe, K.S. (2023). A three-colour stress biosensor reveals multimodal response in single cells and spatiotemporal dynamics of biofilms. *NPJ Biofilms Microbiomes* **9**, 57. <https://doi.org/10.1038/s41522-023-00424-1>.
26. Klumpp, S., Zhang, Z., and Hwa, T. (2009). Growth rate-dependent global effects on gene expression in bacteria. *Cell* **139**, 1366–1375. <https://doi.org/10.1016/J.CELL.2009.12.001>.
27. Deris, J.B., Kim, M., Zhang, Z., Okano, H., Hermesen, R., Groisman, A., and Hwa, T. (2013). The innate growth bistability and fitness landscapes of antibiotic-resistant bacteria. *Science* **342**, 1237435. <https://doi.org/10.1126/science.1237435>.
28. Choudhary, D., Lagage, V., Foster, K.R., and Uphoff, S. (2023). Phenotypic heterogeneity in the bacterial oxidative stress response is driven by cell-cell interactions. *Cell Rep.* **42**, 112168. <https://doi.org/10.1016/J.CELREP.2023.112168>.
29. Jo, J., Price-Whelan, A., and Dietrich, L.E.P. (2022). Gradients and consequences of heterogeneity in biofilms. *Nat. Rev. Microbiol.* **20**, 593–607. <https://doi.org/10.1038/S41579-022-00692-2>.
30. Seaver, L.C., and Imlay, J.A. (2001). Hydrogen peroxide fluxes and compartmentalization inside growing *Escherichia coli*. *J. Bacteriol.* **183**, 7182–7189. <https://doi.org/10.1128/JB.183.24.7182-7189.2001>.
31. Kim, S.O., Merchant, K., Nudelman, R., Beyer, W.F., Keng, T., DeAngelo, J., Hausladen, A., and Stamler, J.S. (2002). OxyR: A molecular code for redox-related signaling. *Cell* **109**, 383–396. [https://doi.org/10.1016/S0092-8674\(02\)00723-7](https://doi.org/10.1016/S0092-8674(02)00723-7).
32. Storz, G., and Tartaglia, L.A. (1992). OxyR: a regulator of antioxidant genes. *J. Nutr.* **122**, 627–630. https://doi.org/10.1093/jn/122.suppl_3.627.
33. Imlay, J.A. (2013). The molecular mechanisms and physiological consequences of oxidative stress: lessons from a model bacterium. *Nat. Rev. Microbiol.* **11**, 443–454. <https://doi.org/10.1038/nrmicro3032>.
34. Imlay, J.A. (2015). Transcription Factors That Defend Bacteria Against Reactive Oxygen Species. *Annu. Rev. Microbiol.* **69**, 93–108. <https://doi.org/10.1146/ANNUREV-MICRO-091014-104322>.
35. Imlay, J.A. (2008). Cellular defenses against superoxide and hydrogen peroxide. *Annu. Rev. Biochem.* **77**, 755–776. <https://doi.org/10.1146/ANNUREV.BIOCHEM.77.061606.161055>.
36. Seo, S.W., Kim, D., Szubin, R., and Palsson, B.O. (2015). Genome-wide Reconstruction of OxyR and SoxRS Transcriptional Regulatory Networks under Oxidative Stress in *Escherichia coli* K-12 MG1655. *Cell Rep.* **12**, 1289–1299. <https://doi.org/10.1016/J.CELREP.2015.07.043>.

37. Sen, A., Zhou, Y., and Imlay, J.A. (2020). During Oxidative Stress the Clp Proteins of *Escherichia coli* Ensure that Iron Pools Remain Sufficient To Reactivate Oxidized Metalloenzymes. *J. Bacteriol.* 202, e00235-20. <https://doi.org/10.1128/jb.00235-20>.
38. Liu, Y., Bauer, S.C., and Imlay, J.A. (2011). The YaaA protein of the *Escherichia coli* OxyR regulon lessens hydrogen peroxide toxicity by diminishing the amount of intracellular unincorporated iron. *J. Bacteriol.* 193, 2186–2196. <https://doi.org/10.1128/JB.00001-11>.
39. Varghese, S., Wu, A., Park, S., Imlay, K.R.C., and Imlay, J.A. (2007). Submicromolar hydrogen peroxide disrupts the ability of Fur protein to control free-iron levels in *Escherichia coli*. *Mol. Microbiol.* 64, 822–830. <https://doi.org/10.1111/J.1365-2958.2007.05701.X>.
40. Jang, S., and Imlay, J.A. (2010). Hydrogen peroxide inactivates the *Escherichia coli* Isc iron-sulphur assembly system, and OxyR induces the Suf system to compensate. *Mol. Microbiol.* 78, 1448–1467. <https://doi.org/10.1111/J.1365-2958.2010.07418.X>.
41. Mancini, S., and Imlay, J.A. (2015). The induction of two biosynthetic enzymes helps *Escherichia coli* sustain heme synthesis and activate catalase during hydrogen peroxide stress. *Mol. Microbiol.* 96, 744–763. <https://doi.org/10.1111/MMI.12967/SUPPINFO>.
42. Mishra, S., and Imlay, J. (2012). Why do bacteria use so many enzymes to scavenge hydrogen peroxide? *Arch. Biochem. Biophys.* 525, 145–160. <https://doi.org/10.1016/J.ABB.2012.04.014>.
43. Seaver, L.C., and Imlay, J.A. (2001). Alkyl hydroperoxide reductase is the primary scavenger of endogenous hydrogen peroxide in *Escherichia coli*. *J. Bacteriol.* 183, 7173–7181. <https://doi.org/10.1128/JB.183.24.7173-7181.2001>.
44. Dubbs, J.M., and Mongkolsuk, S. (2012). Peroxide-sensing transcriptional regulators in bacteria. *J. Bacteriol.* 194, 5495–5503. <https://doi.org/10.1128/JB.00304-12>.
45. Kiley, P.J., and Storz, G. (2004). Exploiting Thiol Modifications. *PLoS Biol.* 2, e400. <https://doi.org/10.1371/JOURNAL.PBIO.0020400>.
46. Ritz, D., Patel, H., Doan, B., Zheng, M., Åslund, F., Storz, G., and Beckwith, J. (2000). Thioredoxin 2 Is Involved in the Oxidative Stress Response in *Escherichia coli*. *J. Biol. Chem.* 275, 2505–2512. <https://doi.org/10.1074/JBC.275.4.2505>.
47. Manchado, M., Michán, C., and Pueyo, C. (2000). Hydrogen Peroxide Activates the SoxRS Regulon In Vivo. *J. Bacteriol.* 182, 6842–6844. <https://doi.org/10.1128/JB.182.23.6842-6844.2000>.
48. Zheng, M., Wang, X., Templeton, L.J., Smulski, D.R., LaRossa, R.A., and Storz, G. (2001). DNA microarray-mediated transcriptional profiling of the *Escherichia coli* response to hydrogen peroxide. *J. Bacteriol.* 183, 4562–4570. <https://doi.org/10.1128/jb.183.15.4562-4570.2001>.
49. Gama-Castro, S., Rinaldi, F., López-Fuentes, A., Balderas-Martínez, Y.I., Clematide, S., Ellendorff, T.R., Santos-Zavaleta, A., Marques-Madeira, H., and Collado-Vides, J. (2014). Assisted curation of regulatory interactions and growth conditions of OxyR in *E. coli* K-12. Database (Oxford) 2014, bau049. <https://doi.org/10.1093/DATABASE/BAU049>.
50. Müller, K., Matzanke, B.F., Schünemann, V., Trautwein, A.X., and Hantke, K. (1998). FhuF, an iron-regulated protein of *Escherichia coli* with a new type of [2Fe-2S] center. *Eur. J. Biochem.* 258, 1001–1008. <https://doi.org/10.1046/J.1432-1327.1998.2581001.X>.
51. Chiancone, E., and Ceci, P. (2010). The multifaceted capacity of Dps proteins to combat bacterial stress conditions: Detoxification of iron and hydrogen peroxide and DNA binding. *Biochim. Biophys. Acta* 1800, 798–805. <https://doi.org/10.1016/J.BBAGEN.2010.01.013>.
52. De Martino, M., Ershov, D., van den Berg, P.J., Tans, S.J., and Meyer, A.S. (2016). Single-Cell Analysis of the Dps Response to Oxidative Stress. *J. Bacteriol.* 198, 1662–1674. <https://doi.org/10.1128/JB.00239-16>.
53. Zhao, G., Ceci, P., Ilari, A., Giangiacomo, L., Laue, T.M., Chiancone, E., and Chasteen, N.D. (2002). Iron and Hydrogen Peroxide Detoxification Properties of DNA-binding Protein from Starved Cells. A ferritin-like DNA-binding protein of *Escherichia coli*. *J. Biol. Chem.* 277, 27689–27696. <https://doi.org/10.1074/JBC.M202094200>.
54. Ravindra Kumar, S.R., and Imlay, J.A. (2013). How *Escherichia coli* Tolerates Profuse Hydrogen Peroxide Formation by a Catabolic Pathway. *J. Bacteriol.* 195, 4569–4579. <https://doi.org/10.1128/JB.00737-13>.
55. Hondorp, E.R., and Matthews, R.G. (2004). Oxidative Stress Inactivates Cobalamin-Independent Methionine Synthase (MetE) in *Escherichia coli*. *PLoS Biol.* 2, e336. <https://doi.org/10.1371/JOURNAL.PBIO.0020336>.
56. Patzer, S.I., and Hantke, K. (2001). Dual repression by Fe²⁺-Fur and Mn²⁺-MntR of the mntH gene, encoding an NRAMP-like Mn²⁺ transporter in *Escherichia coli*. *J. Bacteriol.* 183, 4806–4813. <https://doi.org/10.1128/JB.183.16.4806-4813.2001>.
57. Almeida, C.C., Romão, C.V., Lindley, P.F., Teixeira, M., and Saraiva, L.M. (2006). The role of the hybrid cluster protein in oxidative stress defense. *J. Biol. Chem.* 281, 32445–32450. <https://doi.org/10.1074/JBC.M605888200>.
58. Schembri, M.A., Hjerrild, L., Gjermansen, M., and Klemm, P. (2003). Differential Expression of the *Escherichia coli* Autoaggregation Factor Antigen 43. *J. Bacteriol.* 185, 2236–2242. <https://doi.org/10.1128/JB.185.7.2236-2242.2003>.
59. Wenk, M., Ba, Q., Erichsen, V., MacInnes, K., Wiese, H., Warscheid, B., and Koch, H.G. (2012). A universally conserved ATPase regulates the oxidative stress response in *Escherichia coli*. *J. Biol. Chem.* 287, 43585–43598. <https://doi.org/10.1074/JBC.M112.413070>.
60. Guo, Y., Li, Y., Zhan, W., Wood, T.K., and Wang, X. (2019). Resistance to oxidative stress by inner membrane protein ElaB is regulated by OxyR and RpoS. *Microb. Biotechnol.* 12, 392–404. <https://doi.org/10.1111/1751-7915.13369>.
61. Zaslaver, A., Bren, A., Ronen, M., Itzkovitz, S., Kikoin, I., Shavit, S., Liebermeister, W., Surette, M.G., and Alon, U. (2006). A comprehensive library of fluorescent transcriptional reporters for *Escherichia coli*. *Nat. Methods* 3, 623–628. <https://doi.org/10.1038/nmeth895>.
62. Lagage, V., Chen, V., and Uphoff, S. (2023). Adaptation delay causes a burst of mutations in bacteria responding to oxidative stress. *EMBO Rep.* 24, e55640. <https://doi.org/10.15252/EMBR.202255640>.
63. Ivanova, A., Miller, C., Glinsky, G., and Eisenstark, A. (1994). Role of rpoS (katF) in oxyR-independent regulation of hydroperoxidase I in *Escherichia coli*. *Mol. Microbiol.* 12, 571–578. <https://doi.org/10.1111/J.1365-2958.1994.TB01043.X>.
64. Becker-Hapak, M., and Eisenstark, A. (1995). Role of rpoS in the regulation of glutathione oxidoreductase (gor) in *Escherichia coli*. *FEMS Microbiol. Lett.* 134, 39–44. <https://doi.org/10.1111/J.1574-6968.1995.TB07911.X>.
65. Faulkner, M.J., and Helmann, J.D. (2011). Peroxide Stress Elicits Adaptive Changes in Bacterial Metal Ion Homeostasis. *Antioxid. Redox Signal.* 15, 175–189. <https://doi.org/10.1089/ARS.2010.3682>.
66. Chiang, S.M., and Schellhorn, H.E. (2012). Regulators of oxidative stress response genes in *Escherichia coli* and their functional conservation in bacteria. *Arch. Biochem. Biophys.* 525, 161–169. <https://doi.org/10.1016/J.ABB.2012.02.007>.
67. Cornelis, P., Wei, Q., Andrews, S.C., and Vinckx, T. (2011). Iron homeostasis and management of oxidative stress response in bacteria. *Metallomics* 3, 540–549. <https://doi.org/10.1039/C1MT00022E>.
68. Visick, J.E., and Clarke, S. (1997). RpoS- and OxyR-independent induction of HPI catalase at stationary phase in *Escherichia coli* and identification of rpoS mutations in common laboratory strains. *J. Bacteriol.* 179, 4158–4163. <https://doi.org/10.1128/JB.179.13.4158-4163.1997>.
69. Wei, Q., Le Minh, P.N.L., Dötsch, A., Hildebrand, F., Panmanee, W., Elfarash, A., Schulz, S., Plaisance, S., Charlier, D., Hassett, D., et al. (2012). Global regulation of gene expression by OxyR in an important human opportunistic pathogen. *Nucleic Acids Res.* 40, 4320–4333. <https://doi.org/10.1093/NAR/GKS017>.
70. Barshishat, S., Elgrably-Weiss, M., Edelstein, J., Georg, J., Govindarajan, S., Haviv, M., Wright, P.R., Hess, W.R., and Altuvia, S. (2018). OxyS small RNA induces cell cycle arrest to allow DNA damage repair. *EMBO J.* 37, 413–426. <https://doi.org/10.15252/EMBJ.201797651>.

71. Liang, S.T., Bipatnath, M., Xu, Y.C., Chen, S.L., Dennis, P., Ehrenberg, M., and Bremer, H. (1999). Activities of constitutive promoters in *Escherichia coli*. *J. Mol. Biol.* 292, 19–37. <https://doi.org/10.1006/JMBI.1999.3056>.
72. Choudhary, D., Foster, K.R., and Uphoff, S. (2023). Chaos in a bacterial stress response. *Curr. Biol.* 33, 5404–5414.e9. <https://doi.org/10.1016/J.CUB.2023.11.002>.
73. Tartaglia, L.A., Gimeno, C.J., Storz, G., and Ames, B.N. (1992). Multidegenerate DNA recognition by the OxyR transcriptional regulator. *J. Biol. Chem.* 267, 2038–2045. [https://doi.org/10.1016/s0021-9258\(18\)46050-4](https://doi.org/10.1016/s0021-9258(18)46050-4).
74. Wu, M., Shan, W., Zhao, G.P., and Lyu, L.D. (2022). H₂O₂ concentration-dependent kinetics of gene expression: linking the intensity of oxidative stress and mycobacterial physiological adaptation. *Emerg. Microbes Infect.* 11, 573–584. <https://doi.org/10.1080/22221751.2022.2034484>.
75. Ireland, W.T., Beeler, S.M., Flores-Bautista, E., McCarty, N.S., Röschinger, T., Belliveau, N.M., Sweredoski, M.J., Moradian, A., Kinney, J.B., and Phillips, R. (2020). Deciphering the regulatory genome of *Escherichia coli*, one hundred promoters at a time. *eLife* 9, 1–76. <https://doi.org/10.7554/ELIFE.55308>.
76. Imlay, J.A. (2003). Pathways of Oxidative Damage. *Annu. Rev. Microbiol.* 57, 395–418. <https://doi.org/10.1146/ANNUREV.MICRO.57.030502.090938>.
77. Imlay, J.A., and Linn, S. (1988). DNA damage and oxygen radical toxicity. *Science* 240, 1302–1309. <https://doi.org/10.1126/SCIENCE.3287616>.
78. Park, S., You, X., and Imlay, J.A. (2005). Substantial DNA damage from submicromolar intracellular hydrogen peroxide detected in Hpx- mutants of *Escherichia coli*. *Proc. Natl. Acad. Sci. USA* 102, 9317–9322. <https://doi.org/10.1073/pnas.0502051102>.
79. Åslund, F., Zheng, M., Beckwith, J., and Storz, G. (1999). Regulation of the OxyR transcription factor by hydrogen peroxide and the cellular thiol-disulfide status. *Proc. Natl. Acad. Sci. USA* 96, 6161–6165. <https://doi.org/10.1073/PNAS.96.11.6161>.
80. Schindelin, J., Arganda-Carreras, I., Frise, E., Kaynig, V., Longair, M., Pietzsch, T., Preibisch, S., Rueden, C., Saalfeld, S., Schmid, B., et al. (2012). Fiji: an open-source platform for biological-image analysis. *Nat. Methods* 9, 676–682. <https://doi.org/10.1038/nmeth.2019>.
81. Ollion, J., Elez, M., and Robert, L. (2019). High-throughput detection and tracking of cells and intracellular spots in mother machine experiments. *Nat. Protoc.* 14, 3144–3161. <https://doi.org/10.1038/S41596-019-0216-9>.

STAR★METHODS

KEY RESOURCES TABLE

REAGENT or RESOURCE	SOURCE	IDENTIFIER
Bacterial Strains		
AB1157, $\Delta flhD$, <i>Prna1</i> -mKate2 (SU069)	Choudhary et al. ²⁸	N/A
AB1157, $\Delta flhD$, <i>Prna1</i> -mKate2, (SU069) carrying pUA066- <i>PfhuF</i> -GFPmut2 kan (SU1226)	This study	N/A
AB1157, $\Delta flhD$, <i>Prna1</i> -mKate2, (SU069) carrying pUA066- <i>PfhuC</i> -GFPmut2 kan (SU1221)	This study	N/A
AB1157, $\Delta flhD$, <i>Prna1</i> -mKate2, (SU069) carrying pUA066- <i>PyaaA</i> -GFPmut2 kan (SU1195)	This study	N/A
AB1157, $\Delta flhD$, <i>Prna1</i> -mKate2, (SU069) carrying pUA066- <i>Pdps</i> -GFPmut2 kan (SU1193)	This study	N/A
AB1157, $\Delta flhD$, <i>Prna1</i> -mKate2, (SU069) carrying pUA066- <i>PkatG</i> -GFPmut2 kan (SU1189)	This study	N/A
AB1157, $\Delta flhD$, <i>Prna1</i> -mKate2, (SU069) carrying pUA066- <i>PdsbG</i> -GFPmut2 kan (SU1194)	This study	N/A
AB1157, $\Delta flhD$, <i>Prna1</i> -mKate2, (SU069) carrying pUA066- <i>PznuA</i> -GFPmut2 kan (SU1227)	This study	N/A
AB1157, $\Delta flhD$, <i>Prna1</i> -mKate2, (SU069) carrying pUA066- <i>PmetE</i> -GFPmut2 kan (SU1218)	This study	N/A
AB1157, $\Delta flhD$, <i>Prna1</i> -mKate2, mutL-mYpet, carrying pUA066- <i>PsodA</i> -SCFP3A kan (SU1121)	This study	N/A
AB1157, $\Delta flhD$, <i>Prna1</i> -mKate2, (SU069) carrying pUA066- <i>PoxyR</i> -GFPmut2 kan (SU1217)	This study	N/A
AB1157, $\Delta flhD$, <i>Prna1</i> -mKate2, (SU069) carrying pUA066- <i>PphemH</i> -GFPmut2 kan (SU1188)	This study	N/A
AB1157, $\Delta flhD$, <i>Prna1</i> -mKate2, (SU069) carrying pUA066- <i>PmntR</i> -GFPmut2 kan (SU1223)	This study	N/A
AB1157, $\Delta flhD$, <i>Prna1</i> -mKate2, (SU069) carrying pUA066- <i>PgntP</i> -GFPmut2 kan (SU1219)	This study	N/A
AB1157, $\Delta flhD$, <i>Prna1</i> -mKate2, (SU069) carrying pUA066- <i>PuxuA</i> -GFPmut2 kan (SU1228)	This study	N/A
AB1157, $\Delta flhD$, <i>Prna1</i> -mKate2, (SU069) carrying pUA066- <i>PiscS</i> -GFPmut2 kan (SU1225)	This study	N/A
AB1157, $\Delta flhD$, <i>Prna1</i> -mKate2, (SU069) carrying pUA066- <i>Phcp</i> -GFPmut2 kan (SU1305)	This study	N/A

(Continued on next page)

Continued

REAGENT or RESOURCE	SOURCE	IDENTIFIER
AB1157, $\Delta flhD$, <i>Pma1</i> -mKate2, (SU069) carrying pUA066- <i>Pflu</i> -GFPmut2 kan (SU1308)	This study	N/A
AB1157, $\Delta flhD$, <i>Pma1</i> -mKate2, (SU069) carrying pUA066- <i>PybjC</i> -GFPmut2 kan (SU1307)	This study	N/A
AB1157, $\Delta flhD$, <i>Pma1</i> -mKate2, (SU069) carrying pUA066- <i>PychF</i> -GFPmut2 kan (SU1306)	This study	N/A
AB1157, $\Delta flhD$, <i>Pma1</i> -mKate2, (SU069) carrying pUA066- <i>PyfdL</i> -GFPmut2 kan (SU1304)	This study	N/A
AB1157, $\Delta flhD$, <i>Pma1</i> -mKate2, (SU069) carrying pUA066- <i>PmetR</i> -GFPmut2 kan (SU1220)	This study	N/A
AB1157, $\Delta flhD$, <i>Pma1</i> -mKate2, (SU069) carrying pUA066- <i>PznuC</i> -GFPmut2 kan (SU1224)	This study	N/A
AB1157, $\Delta flhD$, <i>Pma1</i> -mKate2, (SU069) carrying pUA066- <i>PybjN</i> -GFPmut2 kan (SU1303)	This study	N/A
AB1157, $\Delta flhD$, <i>Pma1</i> -mKate2, (SU069) carrying pUA066- <i>PelaB</i> -GFPmut2 kan (SU1311)	This study	N/A
AB1157, $\Delta flhD$, <i>Pma1</i> -mKate2, (SU069) carrying pUA066- <i>Pfur</i> -GFPmut2 kan (SU1192)	This study	N/A
AB1157, $\Delta flhD$, <i>Pma1</i> -mKate2, (SU069) carrying pUA066- <i>PpoxB</i> -GFPmut2 kan (SU1310)	This study	N/A
AB1157, $\Delta flhD$, <i>Pma1</i> -mKate2, (SU069) carrying pUA066- <i>PyaiA</i> -GFPmut2 kan (SU1309)	This study	N/A
AB1157, $\Delta flhD$, <i>Pma1</i> -mKate2, (SU069) carrying pUA066- <i>Pc/pS</i> -GFPmut2 kan (SU1345)	This study	N/A
AB1157, $\Delta flhD$, <i>Pma1</i> -mKate2, (SU069) carrying pUA066- <i>Pc/pX</i> -GFPmut2 kan (SU1346)	This study	N/A
AB1157, $\Delta flhD$, <i>Pma1</i> -mKate2, mutL-mYpet (SU178)	Choudhary et al. ²⁸	N/A
AB1157, $\Delta flhD$, <i>Pma1</i> -mKate2, mutL-mYpet, carrying pUA139 <i>PgrxA</i> -SCFP3A Kan (SU777)	Choudhary et al. ²⁸	N/A
AB1157, $\Delta flhD$, <i>Pma1</i> -mKate2, mutL-mYpet, carrying pUA066- <i>PkatG</i> -SCFP3A kan (SU620)	Choudhary et al. ²⁸	N/A
AB1157, $\Delta flhD$, <i>Pma1</i> -mKate2, mutL-mYpet, carrying pUA066- <i>PahpC</i> -SCFP3A kan (SU948)	Choudhary et al. ²⁸	N/A
AB1157, $\Delta flhD$, <i>Pma1</i> -mKate2, mutL-mYpet Δ KatG (SU590) carrying pUA066- <i>PkatG</i> -SCFP3A kan (SU1325)	This study	N/A
AB1157, $\Delta flhD$, <i>Pma1</i> -mKate2, mutL-mYpet Δ KatG (SU590) carrying pUA066- <i>PgrxA</i> -SCFP3A kan (SU778)	This study	N/A

(Continued on next page)

Continued

REAGENT or RESOURCE	SOURCE	IDENTIFIER
DH5 α , chromosomal <i>PgrxA</i> -SCFP3A-kan (<i>asI</i> A site) (SU1409)	This study	N/A
AB1157, Δ <i>flhD</i> , <i>Prna1</i> -mKate2, (SU069) chromosomal <i>PgrxA</i> -SCFP3A-kan (<i>asI</i> A site) (by P1-phage transduction from SU1409) (SU1410)	This study	N/A
DH5 α carrying pUA066- <i>PkatG</i> -SCFP3 amp (SU1390)	This study	N/A
DH5 α carrying pUA066- <i>PgrxA</i> - SCFP3 amp (SU1392)	This study	N/A
DH5 α carrying pUA066- <i>PkatG</i> -myPet amp (SU1395)	This study	N/A
DH5 α carrying pUA066- <i>PgrxA</i> -myPet amp (SU1394)	This study	N/A
AB1157, Δ <i>flhD</i> , <i>Prna1</i> -mKate2, chromosomal <i>PgrxA</i> -SCFP3A-kan (<i>asI</i> A site) carrying pUA066- <i>PkatG</i> -myPet amp (SU1411)	This study	N/A
AB1157, Δ <i>flhD</i> , <i>P_{RNAI}</i> -mKate2, chromosomal <i>PgrxA</i> -SCFP3A-kan (<i>asI</i> A site) carrying pUA066- <i>PgrxA</i> -myPet amp (SU1412)	This study	N/A
Chemicals, Peptides, and Recombinant Proteins		
M9 minimal salts 5x	Sigma	Product Number: M9956
MEM amino acids	Gibco	Catalog number: 11130-036
L-Proline	Biochemica	Reference Number: A3453,0100
Thiamine	Biochemica	Reference Number: A0955,0050
Pluronic F-127	Sigma	Product Number: P2443-250G
Propidium iodide	Sigma	Product Number: P4170
30% W/W solution of H ₂ O ₂	Sigma	Product Number: H1009-100mL
Kanamycin	Sigma	Product Number: A1493
Agarose	Bio-Rad	Product Number: 1613100
PDMS	Univar Specialty Consumables Ltd	Dowsil / Dow Corning Sylgard 184 Kit 1.1kg
Software and Algorithms		
MATLAB	Mathworks	Mathworks.com
BACMMAN	Schindelin et al., ⁸⁰ Ollion et al. ⁸¹	github.com/jeanollion/bacmman
Python	Spyder	anaconda.com
Deposited Data		
Raw data collected and python code for analysis	This study	Oxford Research Archive - https://ora.ox.ac.uk/objects/uuid:1b2c7733-9fc2-475e-bd15-e4bf1cdc3e39

EXPERIMENTAL MODEL

Strains and plasmids

We used strains derived from *E. coli* K12 AB1157 for our experiments. All the strains had a constitutively expressed *Prna1*-mKate2 marker aiding the segmentation of cells during microscopy and *flhD* deletion to stop the cells from escaping out of the microfluidic growth channels during time-lapse microscopy. The reporter plasmids for genes used in this study were obtained from a transcriptional reporter library of PSC101 plasmids.⁶¹ The reporter plasmids comprised of GFPmut2 fluorescence protein after the promoter region of a given gene or operon and had a kanamycin resistance marker. GFPmut2 was replaced with SCFP3A fluorescent protein for *PkatG*, *PahpC*, and *PgrxA* using Gibson Assembly (NEB).²⁸ The reporter plasmids were mini-prepped and transformed in our AB1157 background strain. Strains were selected on 25 μ g/mL kanamycin resistance LB agarose plates and checked for fluorescence signal by microscopy snapshots.

The chromosomal reporter for *PgrxA*-SCFP3A was constructed by inserting *PgrxA*-SCFP3A-kanamycin using λ -red recombination in endogenous loci (*asfA*) on the chromosome of DH5 α strain carrying pKD46. The successful colonies were selected by growing them overnight at 37C on kanamycin plates and subsequently re-streaking again on kanamycin selective plates to remove the temperature sensitive pKD46 plasmid. Then, the insert was moved into our strain of interest that had *Pma1*-mKate2 marker and *flhD* deletion, using P1 phage transduction. The successful colonies were selected on kanamycin plates and tested for the insert using colony PCR, after which, the colonies were restreaked and grown overnight thrice to remove the phage. Colony PCR was again performed before storing the strain at -80C. *PgrxA*-mYPet and *PkatG*-mYPet plasmids with ampicillin resistance marker were obtained by editing *PgrxA*-SCFP3A and *PkatG*-SCFP3A plasmids using Gibson assembly. We first replaced SCFP3A with mYPet yellow fluorescent protein and the resultant plasmid was edited again using Gibson assembly to replace the kanamycin resistance marker with an ampicillin resistance marker. The final strain was checked by colony PCR, microscopy snapshot, and re-streaking on 100 μ g/mL ampicillin plates. Finally, the *PgrxA*-mYPet and *PkatG*-mYPet plasmids were transformed in the *PgrxA*-SCFP3A chromosomal fluorescent reporter strain to construct the dual reporter strain. The strain was imaged to test for dual fluorescence using microscopy snapshots and selected on plates supplemented with 25 μ g/mL kanamycin and 100 μ g/mL ampicillin.

Media and growth conditions

Strains were stored in 20% glycerol stocks at -80C. Strains were streaked on freshly prepared LB agar plates supplemented with appropriate antibiotics for selection (25 μ g/mL kanamycin and/or 100 μ g/mL ampicillin) and incubated at 37C. One colony was picked from the overnight plates and added in minimal M9 media with appropriate antibiotics for overnight growth at 37C in a shaking incubator at 200rpm. The minimal media was prepared by mixing M9 salts (15 g/L KH₂PO₄, 64 g/L Na₂HPO₄, 2.5 g/L NaCl, and 5.0 g/L NH₄Cl), 2 mM MgSO₄, 0.1 mM CaCl₂, 0.5 mg/mL thiamine, MEM amino acids, 0.1 mg/mL L-proline, and 0.2% glucose. The next day, cells were diluted 1:50 in minimal M9 media and grown for ~3 hours for the microfluidic experiments. 0.85 mg/mL Pluronic F127 was also added to this culture and minimal media to avoid cell aggregation when loading the cells on a microfluidic chip. Minimal media with or without H₂O₂ was flown continuously through microfluidic chips using syringe pumps. The concentration of H₂O₂ used was as specified in the figure legends or text, and was added to the minimal M9 media just before setting up the experiments.

METHOD DETAILS

Microfluidic chip preparation and setup

Microfluidic setup and preparation of ‘mother machine’ devices were performed as described in Choudhary et al.²⁸

Time-lapse microscopy

Time-lapse imaging was performed using a Nikon Ti-E inverted fluorescence microscope equipped with 100x NA 1.40 immersion oil objective, motorized stage, sCMOS camera (Hamamatsu Flash 4), LED excitation source (Lumencor SpectraX), and operated with a perfect focus system. Exposure times were 100 ms for *Pma1*-mKate2 (λ = 555 nm), 300 ms for MutL-mYPet (λ = 508 nm), 75ms for GFPmut2 reporter (λ = 470 nm) and 75 ms for sCFP3 reporter (λ = 440 nm) using 50% of maximal LED excitation intensities. The excitation and emission lights were separated using a triband dichroic and individual emission filters. The microscope chamber (Okolabs) was maintained at 37C throughout the experiments and images were captured every 3 min.

QUANTIFICATION AND STATISTICAL ANALYSIS

Mother machine data processing and analysis

The microscopy time-lapse.nd2 files for the experiments were processed using BACMMAN plugin⁸¹ in Fiji,⁸⁰ which were subsequently analysed using custom made Python scripts. BACMMAN first performs pre-processing which corrects for drifts during imaging and aligns growth channels spatially over time. To obtain cellular parameters, we used the *Pma1*-mKate2 marker to segment and mark the cell outlines against the background and then used this as a mask for other fluorescence channels. In all the fluorescence channels (CFP, GFP and mYPet), the mean fluorescence intensity inside the mask of each cell mask were computed. The cells were tracked over time using the segmentation masks of mKate2 channel to provide cell lineage information. BACMMAN generated output in separate excel files containing cell growth characteristics, *Pma1*-mKate2 intensity data and one file for each fluorescence data. These files were then analyzed using a custom python pipeline to compute cell parameters as described below.

Elongation Rate

The instantaneous elongation rate at time t was calculated based on the log-difference in cell length L_t at time between consecutive frames as $\frac{\log(L_t) - \log(L_{t-\Delta t})}{\Delta t}$. For calculating the elongation rates of cells at different positions in the growth trench, cells were tracked according to their initial position until the number of barrier cells decreased by 2.

Gene expression

Reporter fluorescence intensity values were averaged over the area of each cell.

Number of barrier cells

The number of cells that are located between the open end of a trench and the cell being analysed.

Promoter activity

The instantaneous promoter activity at time t was calculated as the cell averaged rate of change of total fluorescence intensity of a cell. It was computed as¹⁶:

$\frac{1}{A} \frac{d(IA)}{dt} = I \frac{1}{A} \frac{dA}{dt} + \frac{dI}{dt}$ where I is the mean fluorescent intensity of cell and A is the cell area. Here, $\frac{1}{A} \frac{dA}{dt}$ was given by the instantaneous elongation rate of the cell. For calculating the promoter activity values of cells at different positions in the growth trench, cells were tracked according to their initial position until the number of barrier cells decreased by 2.

Expression Rate

The instantaneous expression rate at time t was calculated based on the difference in cell intensity I_t at time between consecutive frames as $\frac{I_t - I_{t-\Delta t}}{\Delta t}$. For calculating the expression rates of cells at different positions in the growth trench, cells were tracked according to their initial position until the number of barrier cells decreased by 2.

Peak expression

90th percentile of the mean fluorescence intensities from 12 to 90 minutes after the start of H_2O_2 treatment.

Steady state expression

Average of the mean fluorescence intensities from 150 minutes after the start of H_2O_2 treatment.

Time to peak expression for single cells

Time in minutes post treatment until 100 minutes when individual cells show maximum fluorescence intensity.

Peak expression for single cells

Mean fluorescence intensity for individual cells from 18 minutes until 90 minutes post treatment. This value was subtracted by the mean fluorescence intensity without H_2O_2 treatment i.e. basal fluorescence intensity.

Coefficient of variation

The CV values were calculated as the standard deviation divided by the mean.

Relative expression in spatial dimension

Expression intensity of cells with at least 1 barrier cells were divided by the intensity of outermost cell (i.e. cell with no barrier cells) for each growth channel at a given time point.

Cross-correlation analysis

The temporal cross-correlation between the different reporter intensity traces of mother cells was computed using the statsmodel library in Python. Correlation values from individual growth trenches were then averaged over all observed growth trenches.

Linear regression analysis

The linear regression analysis was performed in Python using the stats.linregress function in scipy library which computes the least square regression for a linear fit between two sets of data points.

Oxidative stress response model

We modelled the oxidative stress response model as shown in Figure 4A and previously described in Choudhary et al.⁷² Here, external H_2O_2 is provided at the rate R_{influx} . Intracellular H_2O_2 ($[H_2O_2]_{cell}$) oxidises OxyR with rate K_{ox} and converts it to the oxidised form that induces the genes in its regulon. For simplicity, we modelled the induction of important representative genes of the stress response regulon by OxyR: glutaredoxin-1 (grxA) that converts OxyR oxidised back to its reduced form with rate K_{red} , scavengers: alkyl hydroperoxidase (ahpC) and catalase (katG) that reduce $[H_2O_2]_{cell}$ and a reporter gene that does not directly or indirectly affect the OxyR regulation. All gene products are produced at a basal expression rate ($R_{grxA,basal}$, $R_{katG,basal}$, $R_{ahpC,basal}$, $R_{reporter,basal}$) and their expression is modulated upon induction by OxyR. The induction by OxyR is modelled as Michaelis Menten kinetics with maximal induction rate given by K_{ind} ($K_{grxA,ind}$, $K_{ahpC,ind}$, $K_{katG,ind}$, $K_{reporter,ind}$) and half-maximal induction K_m is given by dissociation constant of OxyR from the promoter regions of the genes (K_D) ($K_{D,grxA}$, $K_{D,katG}$, $K_{D,ahpC}$, $K_{D,reporter}$). Finally, the gene expression reduces due to growth dependent dilution effect where growth rate (g) is a function of $[H_2O_2]_{cell}$.

This leads to the following equations:

$$\frac{d[OxyR]_{Red}}{dt} = -K_{ox} \cdot [OxyR_{Red}] \cdot [H_2O_2]_{cell} + K_{red} \cdot [GrxA] \cdot \left(\frac{[OxyR]_{total} - [OxyR]_{Red}}{([OxyR]_{total} - [OxyR]_{Red}) + h_{OxyR}} \right) \quad (\text{Equation 1})$$

$$\frac{d[GrxA]}{dt} = R_{grxA,basal} + K_{grxA,ind} \cdot \left(\frac{[OxyR]_{total} - [OxyR]_{Red}}{([OxyR]_{total} - [OxyR]_{Red}) + K_{D,grxA}} \right) - g \cdot [GrxA] \quad (\text{Equation 2})$$

$$\frac{d[KatG]}{dt} = R_{katG,basal} + K_{katG,ind} \cdot \left(\frac{[OxyR]_{total} - [OxyR]_{Red}}{([OxyR]_{total} - [OxyR]_{Red}) + K_{D,katG}} \right) - g \cdot [KatG] \quad (\text{Equation 3})$$

$$\frac{d[AhpC]}{dt} = R_{AhpC,basal} + K_{AhpC,ind} \cdot \left(\frac{[OxyR]_{total} - [OxyR]_{Red}}{([OxyR]_{total} - [OxyR]_{Red}) + K_{D,AhpC}} \right) - g \cdot [AhpC] \quad (\text{Equation 4})$$

The intracellular $[H_2O_2]_{cell}$ concentration is determined by the influx of external H_2O_2 with rate $R_{influx} \cdot [H_2O_2]_{external}$, a basal endogenous production rate $R_{H_2O_2,basal}$, and scavenging by catalase and peroxidase enzymes with Michaelis-Menten kinetics where K_{AhpC} , K_{KatG} are the catalytic rate constants and h_{AhpC} , h_{KatG} are the Michaelis constants:

$$\frac{d[H_2O_2]_{cell}}{dt} = R_{influx} \cdot [H_2O_2]_{external} + R_{H_2O_2,basal} - K_{AhpC} \cdot [AhpC] \cdot \left(\frac{[H_2O_2]_{cell}}{[H_2O_2]_{cell} + h_{AhpC}} \right) - K_{KatG} \cdot [KatG] \cdot \left(\frac{[H_2O_2]_{cell}}{[H_2O_2]_{cell} + h_{KatG}} \right) \quad (\text{Equation 5})$$

The model was parametrised using the following literature values from Choudhary et al.⁷²:

$$K_{AhpC} = 660 \text{ s}^{-1}, h_{AhpC} = 1.2 \text{ }\mu\text{M}, K_{KatG} = 490000 \text{ s}^{-1}, h_{KatG} = 5900 \text{ }\mu\text{M}$$

$$K_{D,AhpC} = 0.1 \text{ }\mu\text{M}, K_{D,KatG} = 0.18 \text{ }\mu\text{M}, K_{D,GrxA} = 0.1 \text{ }\mu\text{M}, K_{AhpC,act} = 0.2 \text{ }\mu\text{M min}^{-1}, K_{KatG,act} = 0.15 \text{ }\mu\text{M min}^{-1}, K_{GrxA,act} = 0.1 \text{ }\mu\text{M min}^{-1}, R_{grxA,basal} = R_{katG,basal} = 0 \text{ }\mu\text{M min}^{-1}, R_{AhpC,basal} = 0.01 \text{ }\mu\text{M min}^{-1}$$

$$R_{H_2O_2,basal} = 0.02 \text{ }\mu\text{M min}^{-1}, K_{ox} = 0.1 \text{ }\mu\text{M}^{-1} \text{ s}^{-1}, K_{red} = 8 \text{ }\mu\text{M s}^{-1}, h_{OxyR} = 2583 \text{ }\mu\text{M}, [OxyR]_{total} = 1 \text{ }\mu\text{M}, R_{influx} = 1 \text{ min}^{-1}, g = 0.012 \text{ min}^{-1}$$

The following additions were incorporated to our previous model,

A constitutive gene, that is not part of the OxyR regulon, was also modelled such that it was expressed at rate $R_{constitutive}$ and diluted with growth:

$$\frac{d[Constitutive]}{dt} = R_{constitutive} - g \cdot [constitutive] \quad (\text{Equation 6})$$

Here, $R_{constitutive}$ is $0.1 \text{ a.u. min}^{-1}$.

A reporter gene that is regulated by OxyR but does not affect $[H_2O_2]_{cell}$ or OxyR regulation directly, was introduced as follows:

$$\frac{d[reporter]}{dt} = R_{reporter,basal} + K_{reporter,ind} \cdot \left(\frac{[OxyR]_{total} - [OxyR]_{Red}}{([OxyR]_{total} - [OxyR]_{Red}) + K_{D,reporter}} \right) - g \cdot [reporter] \quad (\text{Equation 7})$$

Here $K_{reporter,ind} > 0$ for positive regulation and $K_{reporter,ind} < 0$ for negative regulation.

Here, $R_{reporter,basal} = 4 \text{ a.u. min}^{-1}$ and $K_{reporter,ind} = -30 \text{ min}^{-1} \cdot K_{D,reporter} = -3 \text{ a.u. min}^{-1}$.

To study the effect of K_D and K_{ind} on gene expression dynamics, we varied $K_{D,reporter}$ taking values $0.01 \text{ a.u.}, 0.02 \text{ a.u.}, 0.05 \text{ a.u.}$, keeping $\frac{K_{reporter,ind}}{K_{D,reporter}} = 1$, and we varied $K_{reporter,ind}$ taking values $0.01 \text{ a.u. min}^{-1}, 0.02 \text{ a.u. min}^{-1}, 0.05 \text{ a.u. min}^{-1}$ where $K_{D,reporter}$ was 0.04 a.u.

Lastly, the effect of plasmid copy number variation is considered by modifying the equation for reporter gene expression (Eq 7) such that the gene induction is proportional to the plasmid copy number n . The change in plasmid copy number is computed as a constitutive expression with rate R_n and diluted by cellular growth as given below.

$$\frac{dn}{dt} = R_n - g \cdot n \quad (\text{Equation 8})$$

We took R_n as $0.1 \text{ a.u. min}^{-1}$, and the variation of reporter gene expression on a plasmid is modelled as follows:

$$\frac{d[Reporter]}{dt} = R_{reporter,basal} + K_{reporter,ind} \cdot \left(\frac{[OxyR]_{total} - [OxyR]_{Red}}{([OxyR]_{total} - [OxyR]_{Red}) + K_{D,reporter}} \right) \cdot n - g \cdot [Reporter] \quad (\text{Equation 9})$$

Cell Systems, Volume 15

Supplemental information

**The master regulator OxyR orchestrates bacterial
oxidative stress response genes in space and time**

Divya Choudhary, Kevin R. Foster, and Stephan Uphoff

Supplementary Figures

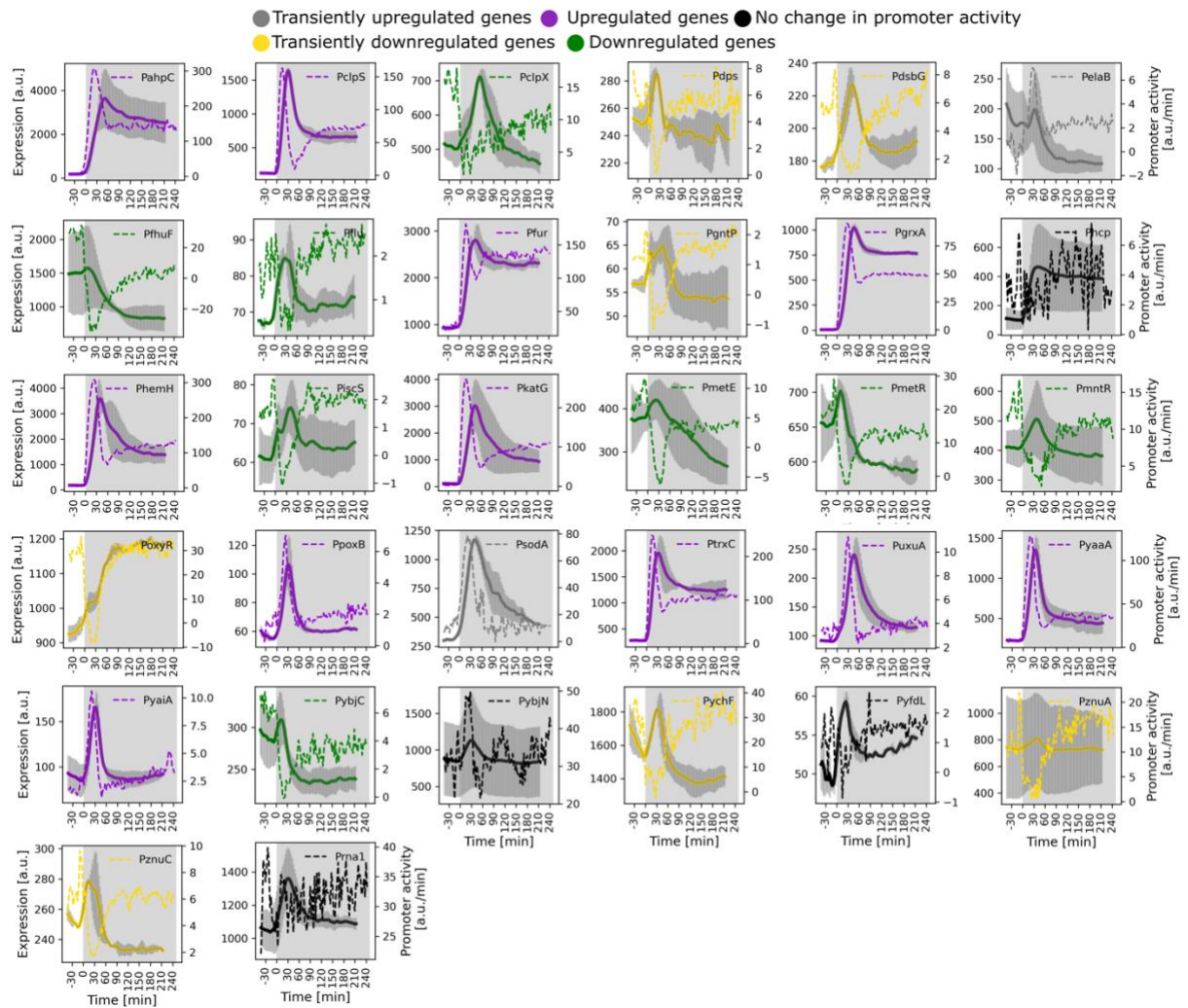


Figure S1: Gene expression dynamics during constant H₂O₂ stress

Mean expression levels (bold) and promoter activity (dash) of frontier cells for 31 transcriptional reporters (ordered alphabetically) and the constitutively expressed promoter *Prna1-mKate2* with constant 100 μ M H₂O₂ treatment from t = 0 minutes (shaded region). Line colours correspond to the gene regulation categories (upregulated :purple, down-regulated: green, transiently up- (grey) or down- (yellow) regulated, no change in promoter activity: black). Error bars represent standard deviation (n \geq 1000 cells and \geq 2 repeats per gene).

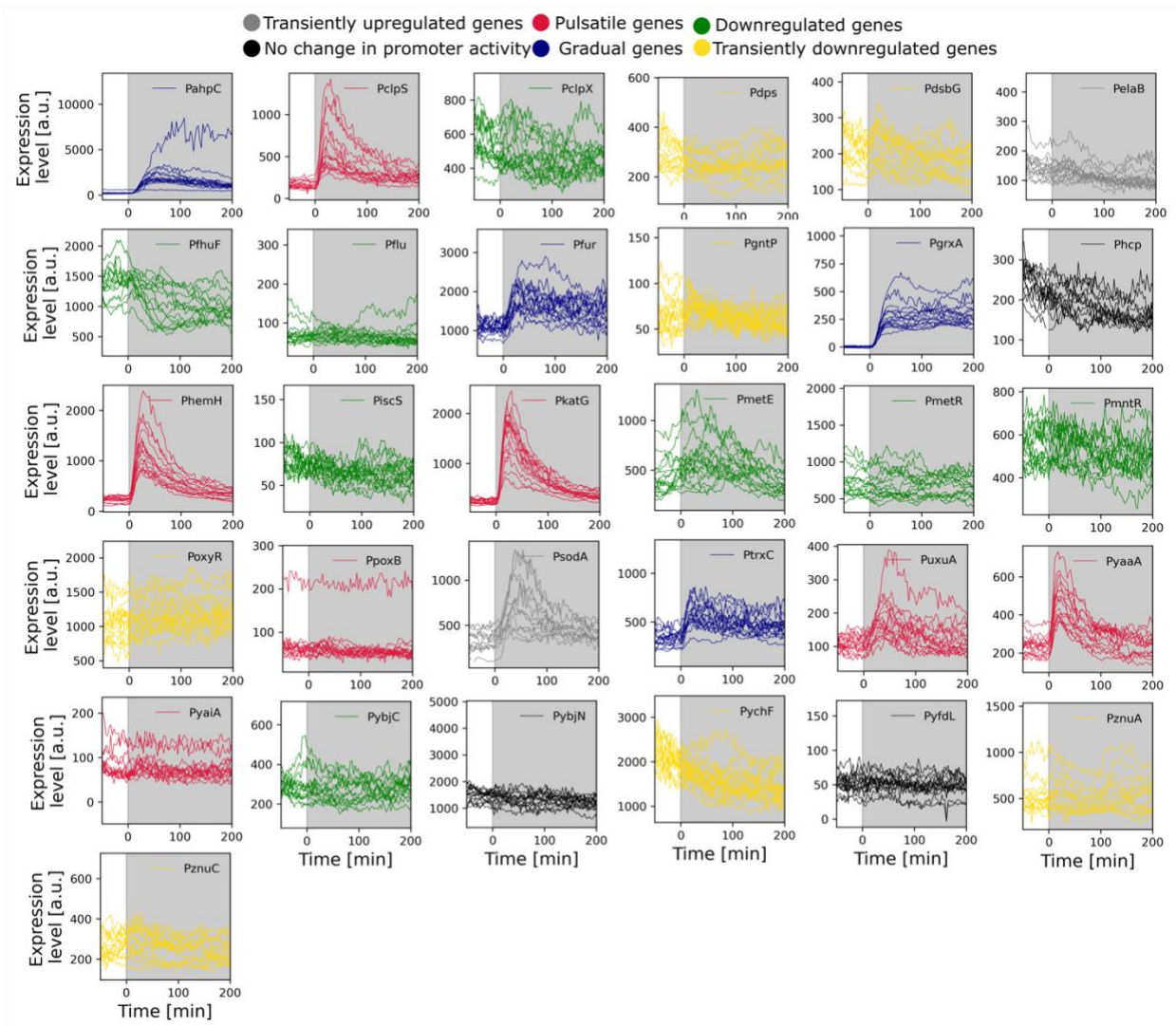


Figure S2: Single cell expression traces of oxidative stress response genes display the cell-cell variability

Single cell expression levels of mother cells for 31 transcriptional reporters with constant 100 μM H_2O_2 treatment from $t = 0$ minutes (shaded region). Line colours correspond to the gene regulation categories (pulsatile: pink, gradual: blue, down-regulated: green, transiently up- (grey) or down- (yellow) regulated, no change in promoter activity: black). $n = 15$ representative traces per gene. Note that the magnitude of the oxidative stress response is substantially lower in mother cells compared to frontier cells. Cells protect each other by actively scavenging local H_2O_2 , creating steep micro-meter scale gradients of oxidative stress response. Consequently, the mother cells experience lower stress levels than frontier cells. Thus, the reduction in growth rate for mother cells is smaller, making the gene expression pulse in mother cells (Figure S2) less pronounced compared to the frontier cells (Figure S1).

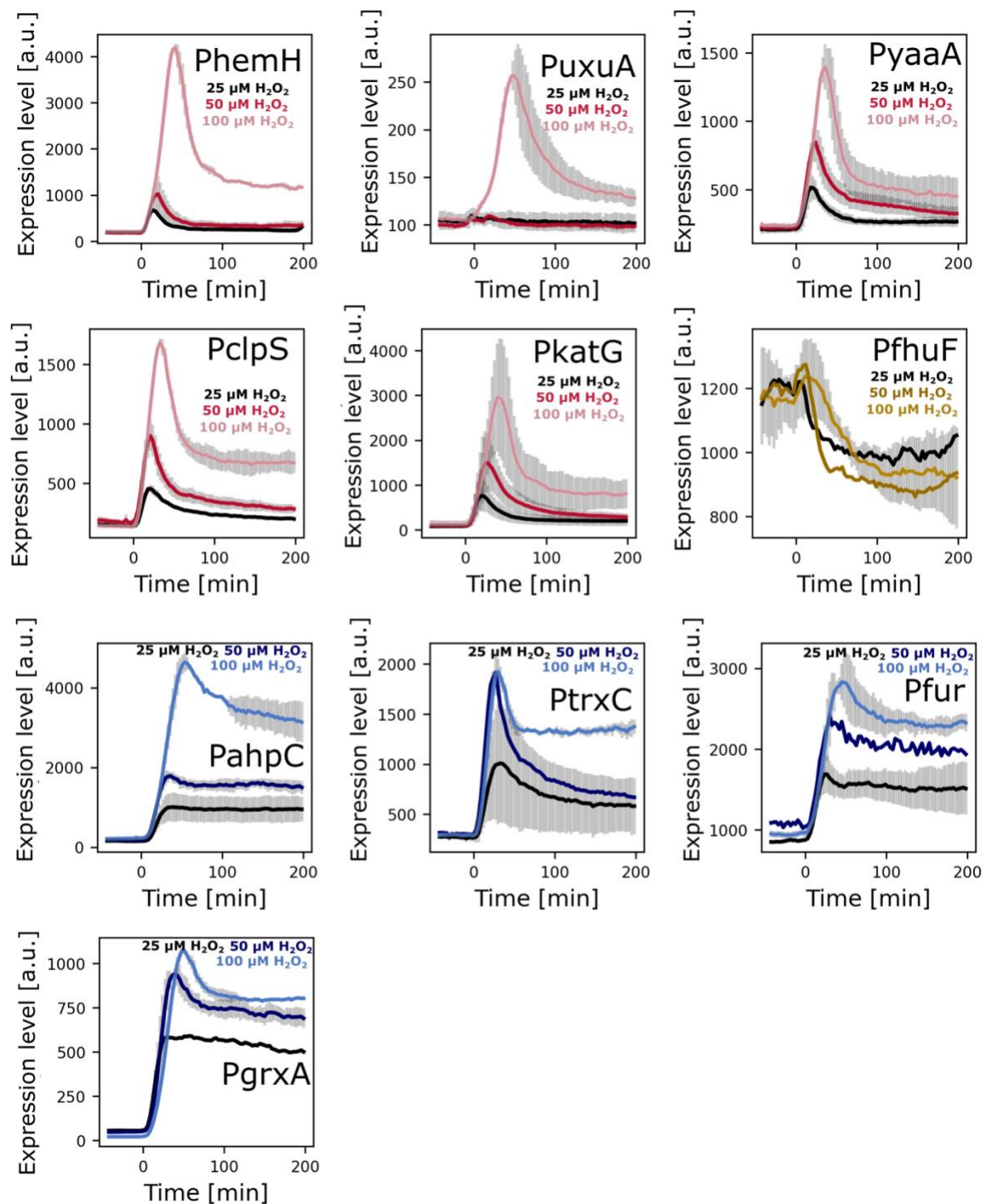


Figure S3: Pulsatile genes exhibit higher expression sensitivity to H_2O_2 stress intensity

Mean expression of frontier cells for the indicated transcriptional reporters under 25 μM , 50 μM and 100 μM H_2O_2 provided from $t = 0$ min (red: pulsatile, blue: gradually responding, yellow: downregulated). Error bars: standard deviation ($n \geq 2$ repeats per gene).

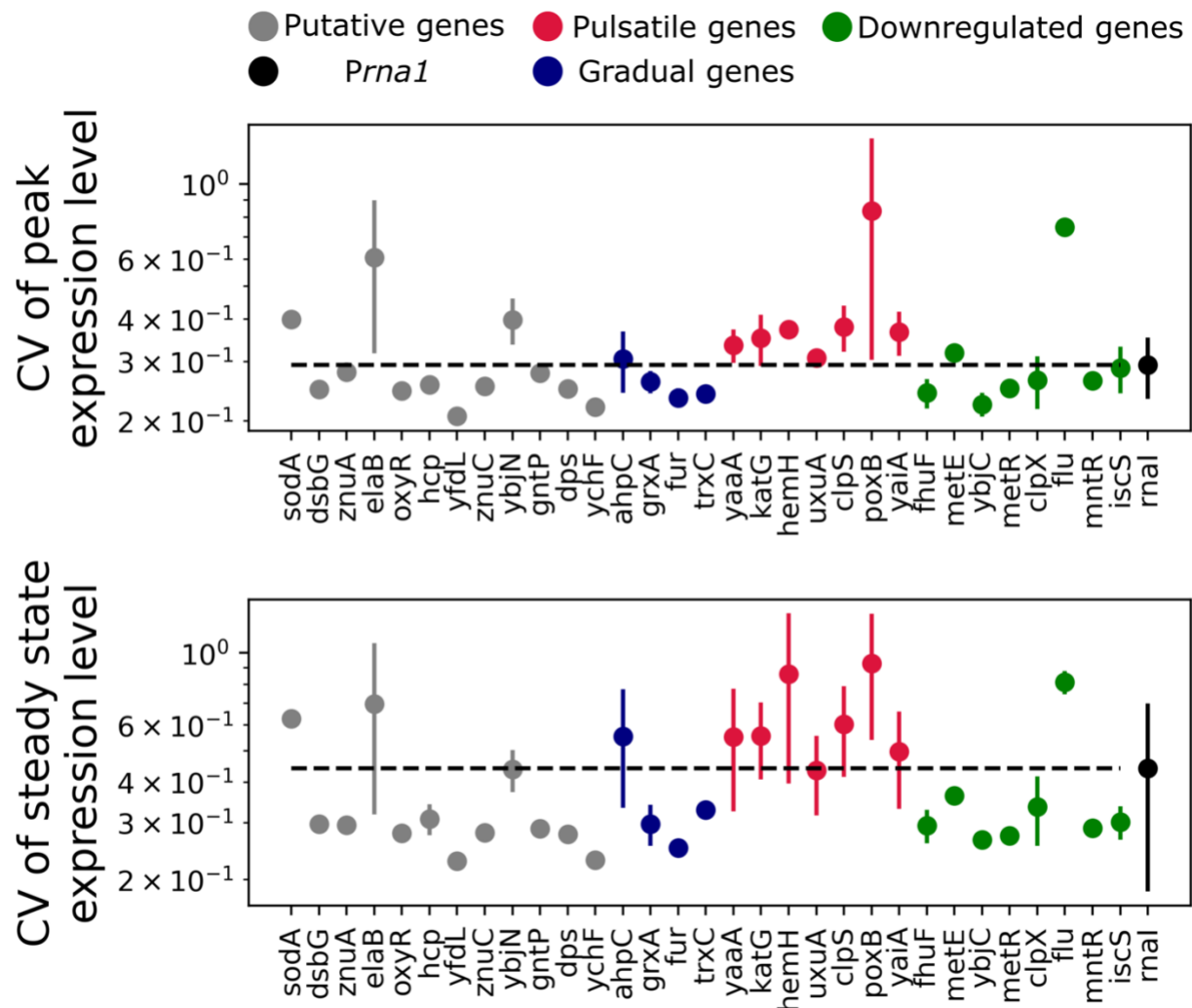


Figure S4: Cell-cell variability in gene expression magnitude for oxidative stress response genes in different regulation categories

Mean coefficient of variation for peak (top) and steady state (bottom) gene expression values for frontier cells under 100 μM H_2O_2 treatment (pulsatile: red, gradual: blue, negative: green, putative: grey, constitutive *Prna1*: black). Error bars represent standard deviation (n ≥ 3 repeats per gene)

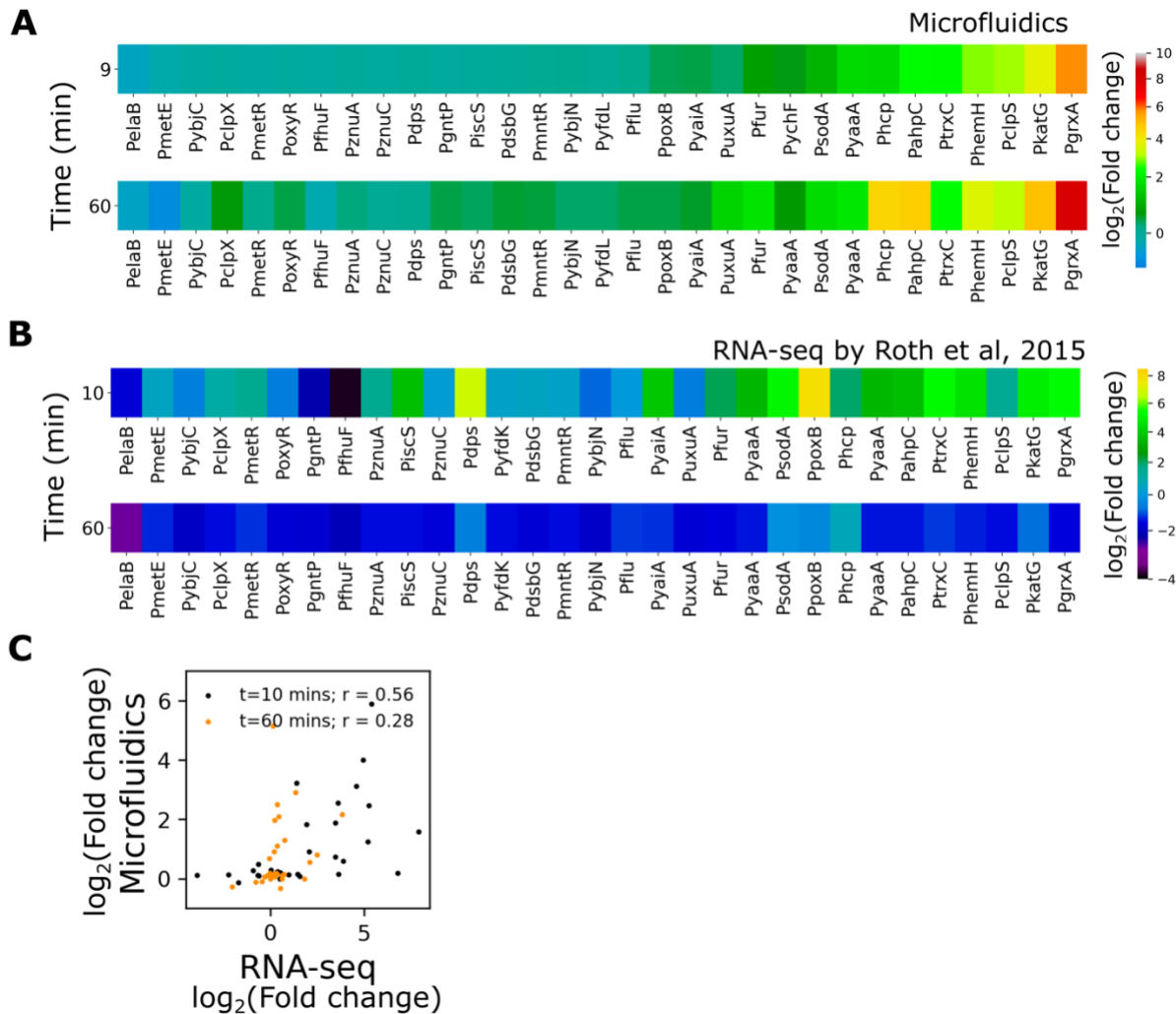


Figure S5: Gene expression level changes in our study compared to the bulk mRNA level changes, reported by Roth *et al.*, under H_2O_2 stress

(A) Heatmap represents mean \log_2 -fold change in gene expression relative to basal level of frontier cells for 31 transcriptional reporters at 9 minutes (top) and 60 minutes (bottom) post treatment with 100 μM H_2O_2 ($n \geq 1000$ cells and ≥ 2 repeats per gene). (B) Heatmap represents data collected by Roth *et al.*⁴, showing mean \log_2 -fold change in mRNA levels of cells for 31 genes at 10 mins (top) and 60 mins (bottom) after treatment with 2.5 mM H_2O_2 . (C) Comparison of \log_2 -fold change in gene expression levels from microfluidic single-cell imaging and mRNA levels in panel A and B at 10 min (black) and 60 minutes (orange) post H_2O_2 treatment. Pearson's coefficient (r) for linear fit between the data sets are indicated in the plot.

Table S1: Genes chosen for this study along with their characteristics.

#	Gene	Function	Implicated in oxidative stress	Regulation in this study (peak /steady-state)	Promoter activity significance value (peak /steady-state)
1	<i>sodA</i>	Superoxide dismutase	P ⁴⁷	P/-	1.72e ⁻⁰⁶ /n.s.
2	<i>fhuF</i>	Ferric iron reductase	N ^{4,48,49}	N/N	2.21e ⁻¹⁸ /2.46e ⁻¹⁰
3	<i>trxC</i>	Thioredoxin 2	P ^{4,36,44-46,48,49}	P/P	2.83e ⁻²³ /2.65e ⁻²⁴
4	<i>yaaA</i>	Suppress intracellular iron levels	P ^{4,38,48}	P/P	2.23e ⁻⁰⁹ /2.0e ⁻¹²
5	<i>dps</i>	Fe-binding & storage	P ^{4,36,49,51,53}	N/-	4.9e ⁻⁰⁵ /n.s.
6	<i>ahpC</i>	Akylhydroperoxidase	P ^{4,36,42,43,48,49}	P/P	1.45e ⁻¹⁷ /4.36e ⁻⁰⁶
7	<i>katG</i>	Catalase	P ^{4,30,36,42,48,49}	P/P	5.24e ⁻²² /2.65e ⁻²⁴
8	<i>grxA</i>	Glutaredoxin-1	P ^{4,36,44,45,49}	P/P	7.029e ⁻¹⁸ /1.18e ⁻¹⁸
9	<i>dsbG</i>	Sulfenic acid reductase	P ^{4,49,54,80}	N/-	1.912e ⁻⁰⁹ /n.s.
10	<i>znuA</i>	Zinc transport	P ³⁶	N/-	7.61e ⁻⁰⁶ /n.s.
11	<i>metE</i>	methionine synthase	P/N ^{36,55}	N/N	3.73e ⁻⁰⁹ /2.31e ⁻⁰⁶
12	<i>oxyR</i>	OxyR	N ^{4,32,49}	N/-	1.512e ⁻⁰⁹ /n.s.
13	<i>hemH</i>	Ferrochelataase	P ^{4,41,48,49}	P/P	7.029e ⁻¹⁸ /1.18e ⁻¹⁸
14	<i>mntR</i>	Mn ²⁺ regulator ⁵⁶	N ^{4,49}	N/N	1.359e ⁻¹⁰ /0.015
15	<i>gntP</i>	gluconate permease	N ^{4,48,49}	N/-	1.512e ⁻⁰⁹ /n.s.
16	<i>uxuA</i>	Mannonate hydrolase	N ^{4,48,49}	P/P	3.36e ⁻⁰⁵ /0.016
17	<i>iscS</i>	Iron-sulfur cluster assembly	N ^{40,48}	N/-	1.29e ⁻⁰⁹ /n.s.
18	<i>hcp</i>	Hybrid cluster proteins of Fe/S	P ^{4,49,57}	-/-	n.s./ n.s.
19	<i>flu</i>	surface adhesin	N/P ^{4,36,49,58}	N/N	0.0076/0.00545

20	<i>ybjC</i>	Unknown	N ^{4,36,48,49}	N/N	1.39e ⁻⁰⁹ /0.00036
21	<i>ychF</i>	ATPase	N ^{4,49,59}	N/-	2.77e ⁻⁰⁶ /n.s.
22	<i>yfdL</i>	Putative ligase	- ⁸⁰	-/-	n.s./ n.s.
23	<i>metR</i>	methionine biosynthesis ⁸¹	P ^{4,36}	N/N	6.046e ⁻⁰⁹ /3.73e ⁻⁰⁶
24	<i>znuC</i>	Zinc transport ⁸²	P ^{4,36}	N/-	1.34e ⁻⁰⁶ /n.s.
25	<i>ybjN</i>	Unknown	N ^{4,49}	-/-	n.s./ n.s.
26	<i>elaB</i>	Membrane integrity	P ^{4,60}	P/P	2.05e ⁻⁰⁵ /n.s.
27	<i>fur</i>	iron-homeostatic control protein	P ^{4,39,48,49}	P/P	2.44e ⁻¹² /5.60e ⁻¹³
28	<i>poxB</i>	pyruvate:quinoneoxidoreductase ⁸³	P ^{4,48}	P/P	8.58e ⁻⁰⁷ /6.17e ⁻⁰⁵
29	<i>yaiA</i>	Unknown	P ^{4,48}	P/P	0.00015/0.00279
30	<i>clpS</i>	Iron sequestration	P ³⁷	P/P	1.3877e ⁻¹³ /1.18e ⁻¹⁸
31	<i>clpX</i>	Iron sequestration	P ³⁷	N/N	1.738e ⁻⁰⁵ /3.67e ⁻⁰⁶

P: upregulation, N: downregulation; p-values using Mann-Whitney tests where n.s. for p>0.05